Highlights

Synchronous median instantaneous power spectrum-gram (SM-IPSgram): A filter banks decomposition for identifying informative frequency band and a weighting function.

Thato Sibanda

- Introduction of the sparsity measure named the spectral log-mean-exp.
- Introduction of the SM-IPSgram for gear diagnostics under harsh operating conditions.
- Identification of the informative frequency band and a weighting function.

Synchronous median instantaneous power spectrum-gram (SM-IPSgram): A filter banks decomposition for identifying informative frequency band and a weighting function.

Thato Sibanda[a,*]

[a]*Centre for Asset Integrity Management, Department of Mechanical and Aeronautical Engineering, University of Pretoria, Pretoria, South Africa*

Abstract

Over the years, *informative frequency band* (IFB) identification emerged with the aim of guaranteeing optimal demodulation-band for the diagnostics of rotating machines. A measured vibration signal from complex rotating machinery, such as a gearbox system, invariantly exhibits heavy and impulsive background noises. As a result, robust IFB identification methods are needed to adapt to these background noises. In this context, a notion of *spectral log-mean-exp* sparsity measure using exponential function-based quasi-arithmetic mean is coined and the *synchronous median instantaneous power spectrum-gram* (SM-IPSgram) is proposed as an IFB identification method for gear diagnostics. The spectral log-mean-exp satisfies at least five of six criteria that are necessary for the measurement of sparsity, and its performance is comparable to that of the classical (but powerful) sparsity measures. On the other hand, the SM-IPSgram has some very attractive properties, viz: (i) it is computationally efficient, (ii) extremely robust, (iii) can cope with all kinds of background noises, e.g. strong cyclostationary interferences, Gaussian and non-Gaussian noise, and (iv) it produces a filter banks decomposition to accentuate only the carrier/spectral frequency of the defect, and thus gives much earlier warning of abnormal conditions. Eventually, the experimental and numerical results are reported to corroborate the effectiveness of the SM-IPSgram, and its intrinsic properties are pointed out and compared to other advanced methods in the literature.

Keywords: Sparsity measures, Spectral log-mean-exp, Gear diagnostics, SM-IPSgram, Weighting function, Informative frequency band

1. Introduction

Gears are vital components in a wide range of industrial and transport applications. A faulty gear system could result in severe damage if defects occur to one of the gears during the operating condition. Many types of gear faults, including fatigue fracture, incipient cracks, and spalls on a tooth face, are localised [1, 2]. As a result, early detection of localised gear faults has been a research imperative for decades. Diagnosing a gear system by examining vibration signals is the most commonly used method for detecting gear failures [3]. Therefore, gear diagnostics is only regarded as meaningful if the damage can be detected at an early stage. Vibration analysis has been widely used in the condition monitoring of rotating machinery [4]. It offers the advantage that accelerometers can be used to acquire the mechanical vibration signals which are representative of physical processes within the gearbox system. Nevertheless, it is still difficult to detect the fault since the signal resulting from the defect is generally obscure [5].

In such a situation, filtering an acceleration signal using an optimal demodulation band may be an indispensable preliminary to gear diagnostics [2, 6, 7]. In the literature, much work has been directed towards the demodulation analysis of signals having time-varying spectral characteristics, and strong background noises [8]. The last decade has seen dramatic advances in the development of *informative frequency band* (IFB) identification methods and their application to machine condition monitoring and fault diagnosis of rotating machinery. The history may conveniently start with the work of Antoni on the method of fast Kurtogram [7] since it was the author who first made effective use of the spectral kurtosis [9, 10] and the 1/3-binary tree filter banks for the automatic identification of optimal demodulation band. The fast Kurtogram in the original paper which forms the basis of all modern research on the subject was applied to diagnose faults under various operating conditions. Spectral kurtosis is the most popular sparsity measure to characterise the sparsity of signals. However, it was shown that spectral kurtosis which is used in the calculation of fast Kurtogram loses effectiveness due to impulsive noise and strong interferences [11]. In more recent years, several consistent estimates of optimal demodulation band have been proposed, each of which exhibits certain advantages over the original one i.e. fast Kurtogram [8, 11–21].

Abbreviations: IFB, informative frequency band; STFT, short-time Fourier transform; SE, squared envelope; IPS, instantaneous power spectrum; SA-IPS, synchronous average instantaneous power spectrum; AIPS, averaged instantaneous power spectrum; CS2, second-order cyclostationary; CIES, combined improved envelope spectrum; TF-IPS, time-frequency instantaneous power spectrum; AF-IPS, angle-frequency instantaneous power spectrum; CS1, first-order cyclostationary; CNS1, first-order cyclo-non-stationary; CNS2, second-order cyclo-non-stationary; FFT, fast Fourier transform; ICS2, indicator of second-order cyclostationary

*Corresponding author.

Email address: matssibanda@gmail.com (Thato Sibanda)

There are many paradigms stemming from diverse research domains advocating the importance of sparsity measures in demodulation analysis. These techniques have been introduced as a premise that permits quantifying the sparsity of signals, and, thus, paving the way to unprecedented possibilities in the fields of machine condition monitoring and fault diagnosis of rotating machinery. The sparse measure is a powerful means to quantify the sparsity of repetitive transients [15] caused by a variety of faults in many types of rotating machinery. Hence, they facilitate the detection of incipient faults and guide optimal envelope demodulation IFB identification. Sparsity measures are based on some commonly used statistical parameters. Currently, the application of these techniques to an angle-time cyclostationary framework offers exciting possibilities for demodulation analysis to enhance the detection of smaller transients [22].

To date, many time-frequency analyses such as the *short-time Fourier transform* (STFT) and the squared envelope (SE) of the complex envelope such as the *instantaneous power spectrum* (IPS) [23] have been used as a basis to identify IFB. The IPS has emerged as a joint time-frequency plane that enables the rapid estimation of instantaneous frequency. However, it is very difficult if not practically impossible to use sparsity measures to identify demodulation bands in the presence of non-Gaussian noise or impulsive interference. In most cases, IFB identification in the presence of non-Gaussian noise and cyclo-stationary interferences is a matter of great difficulty and it is quite impossible to obtain a reliable demodulation band using most existing methods in the literature. Had this been possible, the controversy would long since have been brought to a close.

In the past decades, several extensions of the IPS were proposed which include the *synchronous average instantaneous power spectrum* (SA-IPS). In the literature, Wang and McFadden [24, 25] were the first to introduce the concept of the SA-IPS by calculating the spectrogram from a synchronous averaged signal. Later, Urbanek *et al*. in Ref. [26, 27] presented the concept of the *averaged instantaneous power spectrum* (AIPS) that ties Wang and McFadden approach more closely, but the manner of carrying out the work differed somewhat in details. The AIPS is probably the most significant contribution in the field of gear diagnostics. It has been proved to be a powerful signal processing technique that enables *second-order cyclostationary* (CS2) signals to be separated from the total vibration of the gearbox, and this property makes it very suitable for the detection of vibration transients generated by localised and distributed gear faults. It is particularly useful for analysing the vibration of complex mechanical systems such as gearboxes [24]. However, the very great majority of treatments in the ensuing 10 years used the AIPS only for gear diagnostics, although a few authors do briefly mention how the bearing slip impedes the application of the method for bearing diagnostics. So, when performing any form of synchronised averaging on the bearing signal, we commit an error because the repetitive transients do not correspond to an exact angular position due to the bearing slip [28]. This error is always smaller when the signal is measured under constant operating conditions. While the SA-IPS has proved its performance for gear diagnostics, problems arise when it is applied to vibration signals with strong non-Gaussian noise and interferences. Further investigation thus appeared necessary, and it was clear that it ought to be of a much more robust diagnostic procedure.

This paper concerns the development of IFB identification techniques to perform gear diagnosis of rotating machines. In the last few years, numerous new methods have been proposed to overcome the complexity of the signals generated by complex machines and those generated by faults. The advent of the weighting function to identify multiple filter banks has caused considerable attention to be paid to the development of IFB identification methods that can also be used for that purpose. Hence, the great advances that have been made in IFB identification methods in recent years have been in two directions. On one hand, they are used for the automatic identification of the optimal demodulation band in the presence of strong background noises, and on the other hand, they are used for designing a weighting function or a *Combined Improved Envelope Spectrum* (CIES) to extract multiple filter banks. The purpose of this paper is to contribute to these criteria.

This paper has been organised as follows: Section 2 covers a brief overview of the instantaneous power spectrum, sparsity measures, alpha-stable distribution and gear diagnostics. Section 3 introduces a new concept of spectral log-mean-exp sparsity measure, and the *synchronous median instantaneous power spectrum-gram* (SM-IPSgram) is proposed. Section 4 examine the performance of the spectral log-mean-exp and the SM-IPSgram on the Centre for Asset Integrity Management (C-AIM) experimental datasets in diagnosing the localised gear fault. Their intrinsic properties are clearly pointed out and systematically compared to other methods in the literature. The section ends with a weighting function for identifying multiple IFBs. Section 5 present the phenomenological gearbox model of distributed gear-related faults. Finally, we state in Section 6 some concluding remarks.

2. Preliminaries

This section provides the reader with a short description of existing methods in the literature. First, the Instantaneous power spectrum is described. Then, the concept of sparsity measures, alpha-stable distribution, and gear diagnostics are presented in detail. The concept of sparsity measures has great advantages in providing reliable means of identifying IFB for demodulation analysis. In this paper, sparsity measures will play an important role in developing a robust IFB identification methodology.

2.1. Averaged instantaneous power spectrum

Let $\{x[n]\}_{n=0}^{L_t-1}$ be a discrete record of finite length L_t acquired at the sampling period Δ_t (or sampling frequency Δ_f), having a rotational speed profile $\{\vartheta_s[n]\}_{n=0}^{L_t-1}$ of unit [rad/s]. The STFT transforms a discrete record of finite length into two-dimensional data, with one axis as the location of the tapering data window and the second axis as the corresponding spectral frequency. The spectral

frequency resolution Δf is governed by the uncertainty principle, i.e., inversely proportional to the length of each N_w-long segment. Mathematically, the computation of the STFT or complex envelope is expressed as

$$x(t_m; f_k, \Delta f) = \sum_{n=0}^{N_w-1} x[n + mR_h] \cdot w[n] e^{-2\pi i n k / N_w} \tag{1}$$

where $\Delta f = \Delta_f / N_w$ is the spectral frequency resolution or the bandwidth. The hop size R_h is calculated as an integer of $(1-R_o)N_w$, where N_w is the window length and $R(0 < R \leq 1)$ is the overlap fraction, $i = \sqrt{-1}$, is an imaginary number, $\{x[n + mR]\}_{n=0}^{N_w-1}$ is the shifted version by R_h sample such that it selects N_w-long segment of $\{x[n]\}_{n=0}^{L_t-1}$, and $\{w[n]\}_{n=0}^{N_w-1}$ is a positive-definite N_w-long tapering data window computed from a lag-window (i.e., symmetric about zero). The *time-frequency instantaneous power spectrum* (TF-IPS) can be estimated by the squared envelope of the complex envelope as

$$\varepsilon_x(t_m; f_k, \Delta f) = \frac{\Delta_t}{L_t \sum_{n=0}^{N_w-1} |w[n]|^2} |x(t_m; f_k, \Delta f)|^2 \tag{2}$$

The *angle-frequency instantaneous power spectrum* (AF-IPS) can be calculated by order tracking+ the TF-IPS with respect to the time variable, denoted as

$$\varepsilon_x(\varphi_c; f_k, \Delta f) = COT_{\Delta t \to \Delta \varphi}\{\varepsilon_x(t_m; f_k, \Delta f)\} \tag{3}$$

where $COT_{\Delta t \to \Delta \varphi}\{*\}$ is the computed order tracking transform that converts the time variable t_m at different spectral frequency f_k to an angle variable φ_c. For an angular period of interest ϕ, the averaged instantaneous power spectrum is formally defined as follows [26]:

$$\varepsilon_x^{\phi}(\varphi_a; f_k, \Delta f) = N^{-1} \sum_{n=0}^{N-1} \varepsilon_x(\varphi_a + nL_\varphi; f_k, \Delta f) \tag{4}$$

where L_φ is the angular length of the chosen period and $\varepsilon_x(\varphi_a + nL_\varphi; f_k, \Delta f)$ is the segment of the AF-IPS.

2.2. *Sparsity measures*

This subsection briefly mentions some of the most important blind indicators in the literature of sparsity measures. A number of popular sparsity measures have been reviewed in detail elsewhere (Hurley and Rickard in Ref. [29]).

2.2.1. *Hoyer index*

In statistics, a norm $\|\cdot\|$ is a function that satisfies the following three conditions: relation of scalar multiplication to real multiplication, non-negativity and mapping of the identity, and triangle inequality. In general, norms are defined for matrices and most of them could be defined for vectors. *Hölder norm* is a type of norm, often denoted as $\|\cdot\|_p$ [30]. It is only defined for $p \geq 1$, denoted by, $\|\cdot\|_p = \sqrt[p]{\sum_i |x_i|^p}$, where $|*|$ denotes the symbol of the absolute value of an input signal. We see that $\|\cdot\|_p$ is a non-increasing function of p. In signal processing, Hölder norm is called L_p norm and this is used as a blind indicator for selecting IFB with maximum impulsiveness. There are two commonly used L_p norm vectors and these are: *Manhattan norm* [31], defined as $\|x\|_1 = \sum_i |x_i|$, corresponds to sums of distances along coordinate axes. *Euclidean norm* [32], define as $\|x\|_2 = \sqrt{\sum_i |x_i|^2}$, corresponds to the length of the vector. Therefore, the ratio between the Manhattan norm and the Euclidean norm gives birth to Hoyer index [33]. Its squared envelope [34] is defined as:

$$\text{Hoyer index} = \left(\sqrt{N} - \frac{\sum_{t=0}^{N-1} \varepsilon_x(t; f, \Delta f)}{\sqrt{\sum_{t=0}^{N-1} \varepsilon_x(t; f, \Delta f)^2}} \right) \Big/ \left(\sqrt{N} - 1 \right) \tag{5}$$

where $\varepsilon_x(t; f, \Delta f)$ denote its squared envelope of the complex envelope, for a discrete-time signal $x(t), t = 0, 1, \ldots, N-1$ of length N. The Hoyer index which is simply a normalised version of the ℓ_2/ℓ_1 – norm was proposed by Hoyer [33] in 2004. The Hoyer index which satisfies at least five of six criteria that are necessary for the measurement of sparsity is the second-best sparsity measure after the Gini index and *pq-mean* which satisfies six sparsity measure criteria [29, 35]. However, the mathematical representation of the Gini index deters its use as a sparsity measure since it requires sorting of the value which is challenging. In general, the Hoyer index has more nice properties (i.e. is sensitive to weak fault signatures) and it has been verified to perform better than most sparsity measures.

2.2.2. *Spectral kurtosis*

Kurtosis was first proposed by Karl Pearson [36, 37] in 1905 as a measure of *tailedness* of the probability distribution. In the 1970s, the concept of spectral kurtosis started to develop. In 1983, spectral kurtosis was first used for detecting impulsive events in sonar signals. Two decades later, Antoni and Randall [9, 10] made an extensive investigation on the definition and calculation of spectral kurtosis for condition monitoring of rotating machines to measure the severity of machine faults. In essence, spectral kurtosis calculated from the STFT measures the kurtosis of the modulating signals in the time domain at different spectral frequency bands and is used as a measure of repetitive transients [15] (impulsive and cyclo-stationary in nature). The spectral kurtosis is defined as the fourth-order normalised cumulant [7], given as:

$$K_x(f, \Delta f) = \frac{\left\langle \left| x(t; f, \Delta f) \right|^4 \right\rangle}{\left\langle \left| x(t; f, \Delta f) \right|^2 \right\rangle^2} - 2 \tag{6}$$

where $x(t; f, \Delta f)$ denotes its time-frequency complex envelope in this case is the STFT, f is the spectral frequency, $\Delta f = \Delta_f / N_w$ is the bandwidth or spectral frequency resolution calculated from sampling frequency Δ_f and the window length N_w, $x(t)$ is the time signal for a discrete-time signal $x(t), t = 0, 1, \ldots, N-1$ of length N, and a constant value of negative 2 make use of Fisher's definition (i.e. spectral kurtosis becomes zero for Gaussian noises) to normalise the spectral kurtosis when complex Gaussian noises are considered as an input to spectral kurtosis.

In signal processing, the sparsity measures such as spectral kurtosis are an essential prerequisite for IFB identification methods. Spectral kurtosis is mostly used for STFT-based fast Kurtogram. There exist many other methods that adopted a similar procedure as the fast Kurtogram, but use different sparsity measures or blind indicators.

2.3. *Alpha-stable distribution*

The alpha-stable distribution was first introduced by Lévy [38] in the late 1920s to describe the non-Gaussian (impulsive) behavior in the data. This distribution can be described by four parameters: characteristic exponent α_n, scale parameter or dispersion σ, skewness parameter β and shift parameter μ. It is worth mentioning that the alpha-stable distribution does not have a closed-form probability density function. The characteristic function $\phi_X(u)$ of an alpha-stable distribution [39] can be represented as:

$$\phi_X(u) = \mathbb{E}\{e^{iuX}\} = \begin{cases} \exp\{ -\sigma^{\alpha_n} |u|^{\alpha_n} (1 - i\beta \mathrm{sgn}(u) \tan(\frac{\pi\alpha_n}{2})) + i\mu u \} & \alpha_n \neq 1 \\ \exp\{ -\sigma |u| (1 + i\beta \frac{2}{\pi} \mathrm{sgn}(u) \ln(|u|)) + i\mu u \} & \alpha_n = 1 \end{cases} \tag{7}$$

where the parameters of the distribution are: $\alpha_n \in (0, 2]$ which sets the level of impulsiveness and controls the heaviness of the tail, $\beta \in [-1, +1]$ which determines the degree of symmetry of the distribution, $\sigma > 0$, and $\mu \in \mathbb{R}$. As the characteristic exponent α_n decreases, the corresponding distribution exhibits a power-law behaviour. The alpha-stable distribution reduces to the Gaussian distribution in the case where $\alpha_n = 2$ and $\beta = 0$, [40, 41]. Hence, this distribution can be used on the phenomenological gearbox model to represent both Gaussian and non-Gaussian noise.

2.4. *Gear diagnostics*

The research on gear diagnostics has a significant grounding in literature and industry. The gears are commonly used in many types of rotating machinery to transmit torque from one shaft to another. There are four principal types of gears namely, spur, helical, worm, and bevel gears. The spur gear is one of the simplest types of gear commonly used in many applications to transmit torque between parallel shafts [28]. The teeth of the spur gear are parallel to the shaft which makes the contact ratios lower. The helical gear shares a similar philosophy with the spur gear, but it is less noisy because the teeth are inclined at an angle called helix angle making the contact ratio larger [42]. In contrast, the bevel and worm gears are used to transmit the torque between intersecting and perpendicular shafts respectively [40]. The gears are traditionally thought to be reliable and robust as compared to rolling element bearings, however, the possibility of faults is unavoidable.

The common local gear faults include root cracks, tooth wear, and chipped and broken teeth. These local faults (i.e. CS2 signals) arise periodic shocks over a complete meshing cycle, indicating localised tooth damage. Within a gearbox system, there exist *first-order cyclostationary* (CS1) signals that are deterministic (purely periodic) in nature and are known to be generated by misalignment, shaft unbalance, and gear meshing [43]. Under time-varying operating conditions, these deterministic components and local gear faults become *first-order cyclo-non-stationary* (CNS1) [44] and *second-order cyclo-non-stationary* (CNS2) [45] signals, respectively. As a result, the measured vibration signal is often a mixture of the CNS1 signals, background noise, and CNS2 signals which in combination effectively obscure the CNS2 signals. Since the gears and pinions are phase-locked to shaft speed, their repetitive transients are intrinsically locked to a specific angular period. Hence, they will become CS2 signals after performing angular resampling. In this case, synchronous averaging becomes a powerful tool for enhancing the presence of repetitive transients. A simplified schematic of the gear and pinion meshing is shown in Fig. 1.

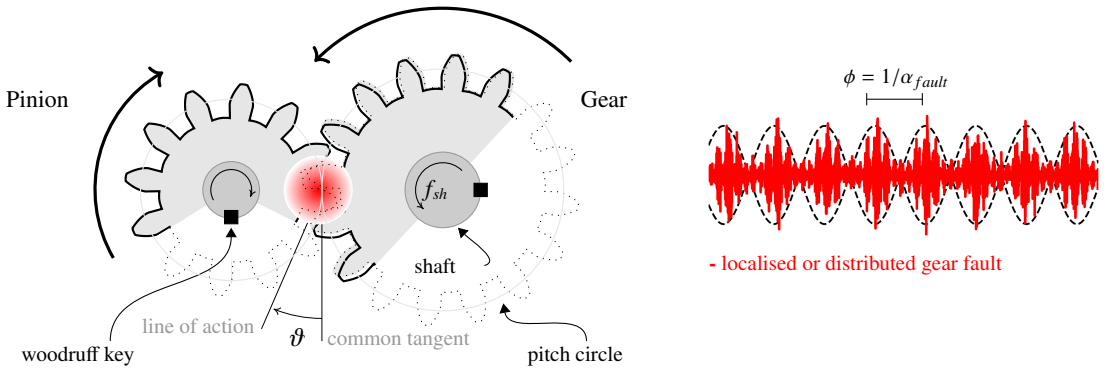

Figure 1: A representation of the localised or distributed gear fault within a gearbox system.

where ϑ is the pressure angle between the common tangent and the line of action (or pressure line) of the pitch circle of gear and pinion, f_{sh} is the shaft frequency, ϕ is the angular period of interest. The pitch circle is the theoretical circle concentric with the axis of the gear and pinion. The woodruff key or simply a shaft key is used for phase-locking the gear or pinion to the shaft. In this case, the gear has 16 teeth, and the pinion has 12 teeth, and thus the gear ratio of this gearbox system is 16/12 = 1.333. The point of engagement shown by the red cycle between the gear and pinion indicates any local gear faults. In signal processing, the majority of work has been conducted on spur gears. The spur gear fault produces noticeable repetitive transients because the small face width results in low contact ratios. The helical gears, on the other hand, have a large face width that results in larger contact ratios, making the fault signatures weaker.

3. Spectral log-mean-exp sparsity measure

This section has three basic purposes: first is to introduce a concept of spectral log-mean-exp; second is to give the mathematically rigorous definitions along with intuitive interpretations of six sparsity measure criteria; third is to illustrate the performance of spectral log-mean-exp and also to give insight into the systematic error or bias associated with unnormalised exponential function and instantaneous energy flow.

3.1. The concept of spectral log-mean-exp

As a classical method to provide a means of identifying IFB for demodulation analysis, sparsity measures have received extensive attention and research in the academic circle. With the rapid evolution of IFB identification methods, the application of sparsity measures has found an increasingly wide utilisation in signal processing and machine learning. In this section, a new concept of spectral log-mean-exp sparsity measure is presented that satisfies five sparsity measure criteria. The spectral log-mean-exp is simply a normalised version of the *exponential function-based quasi-arithmetic mean* (EQAM). Mathematically, the computation of EQAM is formally defined as follows [46]:

$$M_{E^x} = \log_E\left(\sum_{n=0}^{N-1} E^{X_{l,h}[n]}/N\right), \tag{8}$$

where E is a constant and satisfies: $E \in \mathbb{R}^+, E \neq 1$. When E is an exponential function $\exp(\cdot)$, $\log_E(\cdot)$ is equivalent to a natural logarithm, viz: $\log_E(\cdot) = \ln(\cdot)$. $X_{l,h}[n]$ is a bandpass filtered signal obtained by using a bandpass filter with a passband $[l, h]$.

In the diagnostics of rotating machines, the use of EQAM as a sparsity measure is threefold: (i) the exponential function is used to explode (i.e. numbers go from very small to very large very quickly) the time-domain signal, (ii) the mean or average improves the detection of low-impact energy repetitive transients [15], and (iii) the logarithmic function which is the inverse function to exponentiation, is used to remove large values. However, this simple approach is prone to systematic errors and numerical overflow, and thus it cannot provide reliable guidance for identifying optimal demodulation bands.

The exponential function trick [47] for avoiding numerical overflow is given as $\log_E(\sum_{n=0}^{N-1} E^{X_{l,h}[n]-\max\{X_{l,h}[n]\}} \cdot E^{\max\{X_{l,h}[n]\}}/N)$, where $\max\{X_{l,h}[n]\}$, is the shifting to avoid numerical overflow. If $\max\{X_{l,h}[n]\} \in \mathbb{R}$ then, $\log_E(\sum_{n=0}^{N-1} E^{X_{l,h}[n]-\max\{X_{l,h}[n]\}}/N) + \max\{X_{l,h}[n]\}$. Hence, the largest positive exponentiated values boil down to unity, and the other negative exponentiated values boil down to arbitrary infinitesimal positive values. The *spectral log-mean-exp* of a signal $X_{l,h}[n]$ is formally defined as follows:

$$M_{E^x} = \log_E\left(\sum_{n=0}^{N-1} E^{\xi_{l,h}[n]-\max\{\xi_{l,h}[n]\}}/N\right) + \max\{\xi_{l,h}[n]\}, \tag{9}$$

where $\xi_{l,h}[n] = X_{l,h}[n]/\langle X_{l,h}[n]\rangle$ is the energy flow normalised by its averaged value, $\langle X_{l,h}[n]\rangle = \sum_{n=0}^{N-1} X_{l,h}[n]/N$ denote infinite average operation performed over the whole length of a signal. Hence, the spectral log-mean-exp computed from the TF-IPS may be exhibited in the expanded form, denoted as

$$LME_{\varepsilon}(f,\Delta f) = \max\left\{\frac{\varepsilon_x(n;f,\Delta f)}{\langle\varepsilon_x(n;f,\Delta f)\rangle}\right\} + \ln\left(\frac{1}{N}\sum_{n=0}^{N-1}\exp\left(\frac{\varepsilon_x(n;f,\Delta f)}{\langle\varepsilon_x(n;f,\Delta f)\rangle} - \max\left\{\frac{\varepsilon_x(n;f,\Delta f)}{\langle\varepsilon_x(n;f,\Delta f)\rangle}\right\}\right)\right), \tag{10}$$

where $\varepsilon_x(n;f,\Delta f)$, denote the TF-IPS shown in Eq. (2), $\varepsilon_x(n;f,\Delta f)/\langle\varepsilon_x(n;f,\Delta f)\rangle$ is the instantaneous energy flow normalised by its averaged value, $LME_{\varepsilon}(f,\Delta f)$ is the SE spectral log-mean-exp, $\langle\varepsilon_x(n;f,\Delta f)\rangle = \sum_{n=0}^{N-1}\varepsilon_x(n;f,\Delta f)/N$, denote infinite average operation, performed over the whole length of the time signals at different spectral frequencies. The spectral log-mean-exp as a sparsity measure serves to accentuate an optimal demodulation band that can be used to extract the most out of vibration signal, while it is computationally efficient to calculate. This sparsity measure with two normalisations: (i) instantaneous energy flow, and (ii) exponential function, is now sufficiently developed for our purpose.

3.2. Six sparsity measure criteria

Sparse attribute 1 (Robin Hood): *Let* $\mathbf{c} = [c_1, c_2, \ldots, c_n]$, *if* $\mathbf{c}' = [c_1, \ldots, c_i + \alpha, \ldots, c_j - \alpha, \ldots, c_n]$, *then* $\mathbf{S}(\mathbf{c}') < \mathbf{S}(\mathbf{c})$, $\forall\alpha, c_i, c_j \mid c_j > c_i$, $\alpha < (c_j - c_i)/2$, *and* $\alpha \in \mathbb{R}$ *holds. The Robin Hood sparsity measure criteria indicate that the signal sparsity is decreased by subtracting a specific amount from a large coefficient and adding this amount to a smaller coefficient as the energy of the signal spreads out along the coefficients.*

Sparse attribute 2 (Scaling): *Let* $\alpha\mathbf{c} = [\alpha c_1, \alpha c_2, \ldots, \alpha c_n]$, *if* $\mathbf{S}(\alpha\mathbf{c}) = \mathbf{S}(\mathbf{c})$, $\forall\alpha \in \mathbb{R}^+$ *holds. The scaling sparsity measure criteria indicate that multiplying all signal coefficients with the same scalar quantity must not affect signal sparsity. Therefore, it is possible to calculate and compare the sparsity of represented signals with unequal magnitudes in different transform domains.*

Sparse attribute 3 (Rising tide): *Let* $\alpha + \mathbf{c} = [c_1 + \alpha, c_2 + \alpha, \ldots, c_n + \alpha]$, *if* $\mathbf{S}(\alpha + \mathbf{c}) = \mathbf{S}(\mathbf{c})$, $\forall\alpha \in \mathbb{R}^+$ *holds, except for the case where* $c_1 = c_2 = \cdots = c_n$. *The rising tide sparsity measure criteria indicate that signal sparsity is reduced if a scalar quantity is added to each term. Indeed, by adding the same scalar to all coefficients, the relative difference among coefficients becomes negligible and therefore the sparsity should asymptotically become zero.*

Sparse attribute 4 (Cloning): *Let* $\mathbf{c} \parallel \mathbf{c} = [c_1, c2, \ldots, c_n; c_1, c2, \ldots, c_n]$, *if* $\mathbf{S}(\mathbf{c}) = \mathbf{S}(\mathbf{c} \parallel \mathbf{c}) = \mathbf{S}(\mathbf{c} \parallel \mathbf{c} \parallel \mathbf{c}) = \mathbf{S}(\mathbf{c} \parallel \mathbf{c} \cdots \parallel \mathbf{c})$ *holds, where* $\parallel$ *denotes concatenation operation. The cloning sparsity measure criteria indicate that concatenating several signals which comprise exact copies of the original one must not affect signal sparsity. In other words, the sparsity of each signal is equal to the sparsity of a twin signal.*

Sparse attribute 5 (Bill Gates): $\forall i \in \{1, 2, \ldots, n\}$, $\exists\beta = \beta_i > 0$, *such that* $\forall\alpha > 0 : \mathbf{S}([c_1, \ldots, c_i + \beta_i + \alpha, \ldots, c_n]) > \mathbf{S}([c_1, \ldots, c_i + \beta_i, \ldots, c_n])$ *holds. The Bill Gates sparsity measure criteria indicate that by increasing the scalar quantity of a signal coefficient while maintaining the remaining coefficients, the sparsity increases, as the signal energy is concentrated to a mere coefficient.*

Sparse attribute 6 (Babies): *Let* $\mathbf{c} \parallel 0 = [c_1, c2, \ldots, c_n; 0, 0, \ldots, 0]$, *if* $\mathbf{S}(\mathbf{c} \parallel 0) > \mathbf{S}(\mathbf{c})$ *holds. The Babies sparsity measure criteria indicate that by adding extra zeros to the original signal, the signal sparsity increases. This criterion has a similar effect to Bill Gates's sparse attribute since adding zeros increases the signal energy concentration to fewer coefficients.*

Table 1: Six sparsity measure criteria (Robin Hood, Scaling, Rising Tide, Cloning, Bill Gates, and Babies) for exponential function-based quasi-arithmetic mean and spectral log-mean-exp.

Sparsity measures	Definition	C1	C2	C3	C4	C5	C6
Exponential function-based quasi-arithmetic mean (EQAM)	$\log_E\left(\sum_{n=0}^{N-1} E^{X_{l,h}[n]}/N\right)$	✓	✗	✗	✗	✓	✓
Spectral Log-mean-exp	$\log_E\left(\sum_{n=0}^{N-1} E^{\xi_{l,h}[n]-\max\{\xi_{l,h}[n]\}}/N\right)+\max\{\xi_{l,h}[n]\}$, where $\xi_{l,h}[n] = X_{l,h}[n]/\langle X_{l,h}[n]\rangle$	✓	✓	✓	✗	✓	✓

For the sake of simplicity, we confine ourselves almost entirely to a few sparsity measures related to exponential function-based quasi-arithmetic mean. It is proved mathematically in Table 1 that the spectral log-mean-exp satisfies five sparsity measure criteria (Robin Hood, Scaling, Rising Tide, Bill Gates, and Babies). These criteria have demonstrated the major effectiveness and adequacy of the spectral log-mean-exp compared with the exponential function-based quasi-arithmetic mean which satisfied only three sparsity measure criteria (Robin Hood, Bill Gates, and Babies).

3.3. Examples of application

The usefulness of spectral log-mean-exp as sparsity measures for demodulation analysis is investigated. To demonstrate the systematic error or bias associated with unnormalised energy flow, the EQAM and spectral log-mean-exp are computed and displayed in Fig. 2. The TF-IPS used to compute the spectral log-mean-exp was calculated from the acceleration signal obtained from the C-AIM experiment datasets which will be described in detail in Section 5.1. Experimental results for EQAM sparsity measures (see Figs. 2(a) and 2(c)) indicate that the EQAM perform sub-optimally since it introduces too much discordant that will hinder it to provide a means of paving a binary tree filter banks for identifying optimal demodulation band.

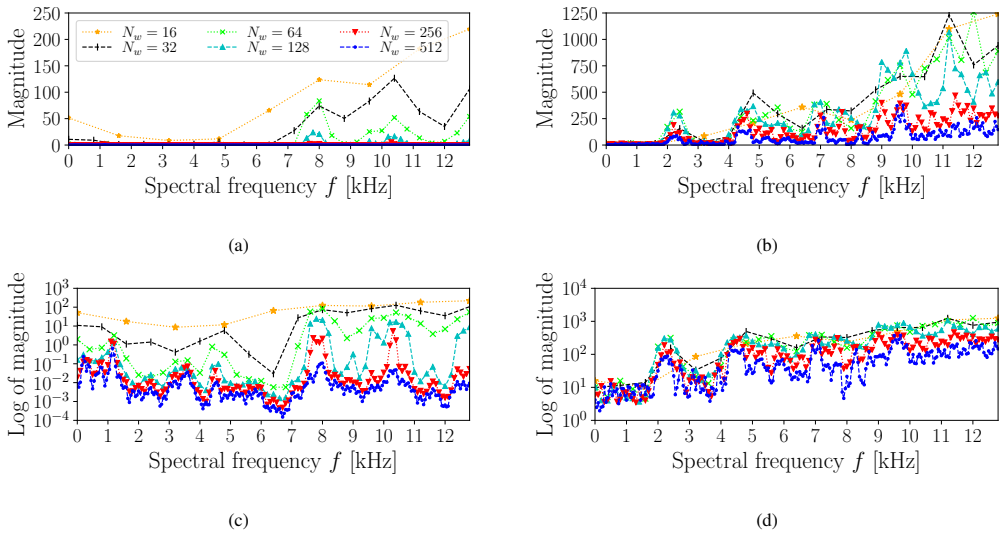

Figure 2: Exponential function-based quasi-arithmetic mean (EQAM) with unnormalised instantaneous energy flow and unnormalised instantaneous energy flow in logarithmic scale (subplot (a) and (c) respectively) and the spectral log-mean-exp with normalised instantaneous energy flow and normalised instantaneous energy flow in logarithmic scale (subplot (b) and (d) respectively).

The experimental results for spectral log-mean-exp sparsity measure are illustrated in Figs. 2(b) and 2(d). The preceding results proved that the spectral log-mean-exp exhibits reliable sparse quantisation capability as compared with the EQAM sparsity measure. In particular, the normalised sparsity measures obey the central limit theorem because the spectral log-mean-exp at different window lengths tends to a normal distribution. If such an estimate obeys the Central Limit Theorem, then the smaller and larger window lengths tend to contain minimal impulsiveness.

In order to demonstrate the numerical overflow associated with an unnormalised exponential function, the spectral log-mean-exp for unnormalised and normalised exponential functions using a window length of 64 and 128 are computed and displayed in Figs. 3(a) and 3(b) respectively.

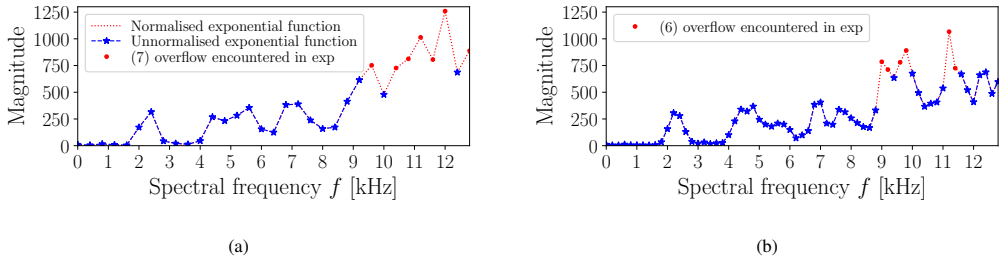

Figure 3: Sparsity measure: the spectral Log-mean-exp with normalised exponential function and unnormalised exponential function with overflow encountered when exponentiating a value greater than or equal to 710 in magnitude: (a) computed from the IPS with the window length of $N_w = 64$, and (b) computed from the IPS with the window length of $N_w = 128$.

In order to get an exact idea of how numerical overflow affects the performance of the unnormalised exponential function of the spectral log-mean-exp, it is necessary to examine in detail the sparsity measure on the SE of the complex envelope with substantially large magnitude, so that we can show the magnitude under which the numerical overflow is encountered in the exponential function. From the preceding results, it is apparent that the magnitude greater than exp(710) = ∞, will lead to numerical overflow to be

encountered in the exponential function and *vise versâ*. One can distinguish between different normalised and unnormalised exponential functions of the spectral log-mean-exp. In this way, we can guard against the numerical overflow related to the exponential function. The utility of this sparsity measure will appear more clearly in the ensuing sections.

4. Proposed methodology

This subsection presents the state of the art regarding the IFB identification method named the SM-IPSgram. In detail the SM-IPSgram for identifying the IFB and a weighting function is specially designed to enable pervasive monitoring of rotating machinery under harsh operating conditions, thus allowing the detection of gear faults at an incipient stage. The performance of the proposed method is reliant on the sparsity measures, viz., the spectral log-mean-exp. In order to decide what conventional binary tree filter banks are to be attached to our proposed SM-IPSgram, it seems necessary in the first instance to consider the 1/2-binary tree as it is the simplest and most cost-effective, we then consider the filter bands of the 1/3-binary tree. The flow diagram for SM-IPSgram is shown in Fig. 4 and the step-by-step details for its extraction are described as follows.

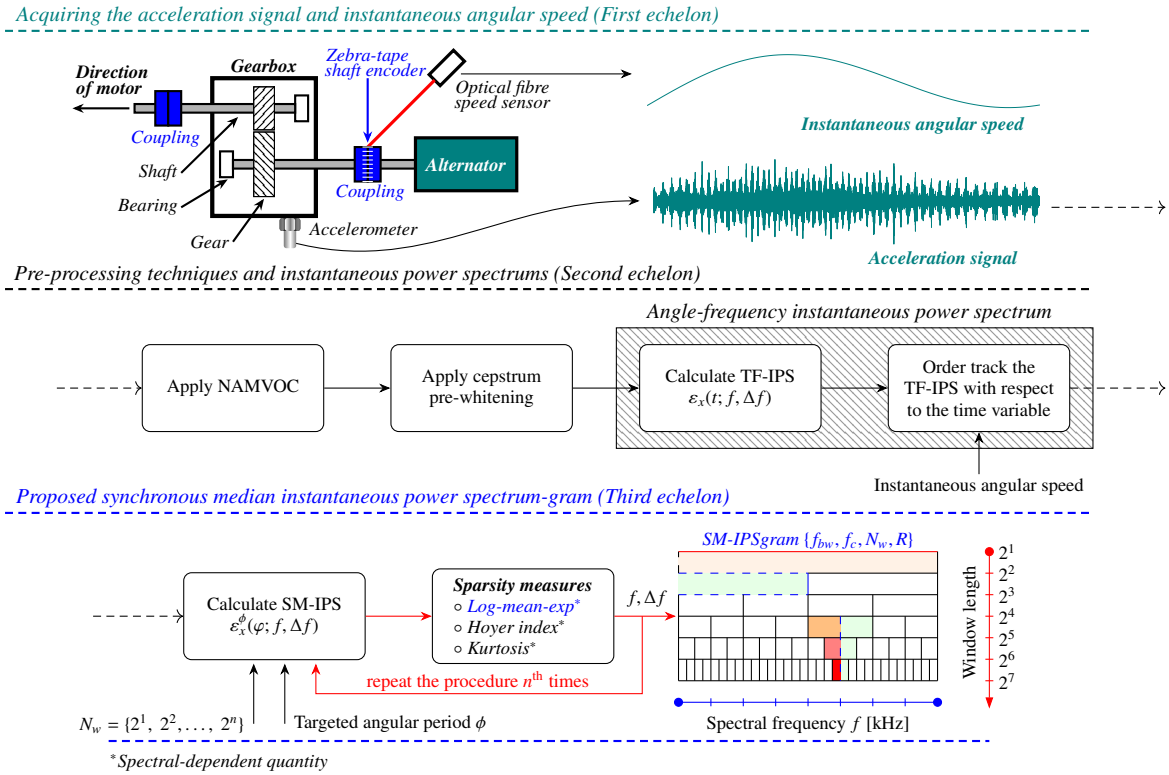

Figure 4: A three-echelon flow diagram comprised of (i) acquiring the acceleration signal and instantaneous angular speed, (ii) pre-processing techniques and instantaneous power spectrums, and (iii) the proposed synchronous median instantaneous power spectrum-gram. As indicated by the dashed arrow lines, the second and third echelons are the continuation of the first and second echelons, respectively.

Step 1. Measure the vibration signal from the rotating machinery and remove the amplitude modulations using NAMVOC [48]. This changes the CNS1 signals into CS1 signals under time-varying operating conditions. Then, remove these CS1 signals or deterministic gear components using the cepstrum pre-whitening.

Step 2. Calculate the whitened TF-IPS, $\varepsilon_x(t; f, \Delta f)$, then order tracked it with respect to the time axis to yield AF-IPS, $\varepsilon_x(\varphi; f, \Delta f)$.

Step 3. Apply synchronous median (SM) to a whitened AF-IPS with respect to angle φ axis at a targeted angular period $\phi = \alpha_{fault}^{-1}$ to yield a whitened SM-IPS, $\varepsilon_x^{\phi}(\varphi; f, \Delta f)$.

Step 4. In this step, the sparsity measures are applied to whitened SM-IPS with respect to angular position φ axis to yield a spectral frequency vector $(f, \Delta f)$ that contains rich information about the impulsiveness of the enhanced modulating signals on the whitened SM-IPS. This procedure is repeated n^{th} times, where n ranges from 1 to $\lfloor \log_2(\text{length}(x(t))) \rfloor$, with an increment of 1 for 1/2-binary tree filter banks. The overlap fraction R is set to a constant value of 0.75 for the SM-IPSgram.

Step 5. Lastly, we use the IFB, $[f_{bw}, f_c]$, and the spectral frequency vector $(f, \Delta f)$ on the SM-IPSgram corresponding to N_w to design the weighting function, $\omega_f(f, \Delta f)$ that is used to combine multiple IFBs.

5. Experimental investigations

This section aims to assess and compare the detection and diagnostic capability of the SM-IPSgram estimation of the spectral log-mean-exp to other advanced methods in the literature, on the basis of the experimental results. In Section 5.3, we demonstrate the superiority of the SM-IPSgram in identifying optimal demodulation band of the localised gear fault over two competing methods, namely the fast Kurtogram, and the ICS2gram. The selection of these methods is based on their advanced performance and historical importance in this field of study. The fast Kurtogram is simpler and will be considered first. In the literature, the fast Kurtogram has been used as a benchmark for the IFB selection to obtain a rich filter band blindly. On the other hand, the ICS2gram has the potential to reveal weak faults more effectively because it uses an *indicator of second-order cyclostationary* (ICS2) content [49] as an objective function.

5.1. The C-AIM experimental dataset

The gear run-to-failure data provided by the Centre for Asset Integrity Management (C-AIM) at the University of Pretoria in South Africa are used as a benchmark dataset. The helical gearbox test rig was originally designed by Stander and Heyns in Ref. [50]. It mainly consists of an alternator, three helical gearboxes, and an electrical motor. The test rig also consists of a set of vibration acquisition systems, a personal computer, and a control box that cannot be seen in the setup. The two helical gearboxes which are not monitored have the same structure, the one connected with the motor reduces speed and the other one increases speed. The monitored helical gearbox is comprised of bearings, gear, pinion, and shafts. An alternator and electrical motor apply time-varying load and speed to the test rig, respectively. The C-AIM experimental test rig is shown in Fig. 5.

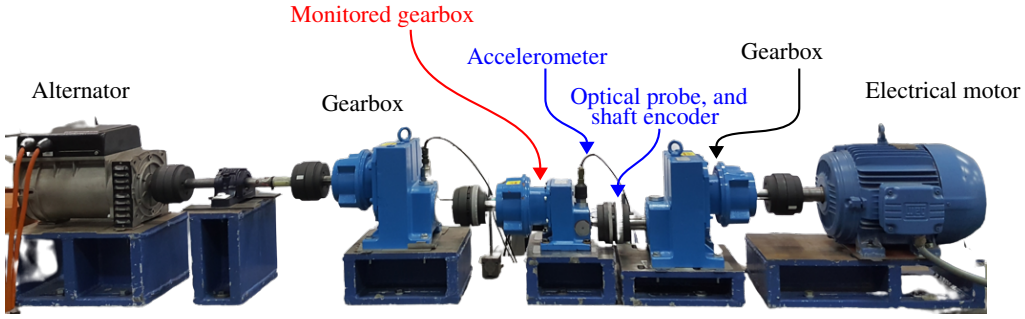

Figure 5: Centre for Asset Integrity Management (C-AIM) experimental test rig [51].

The monitored helical gearbox on the C-AIM experimental test rig is Siemens E68-A-100 helical gearbox, and the other two gearboxes are Siemens E38-A-100 helical gearboxes. The motor is Weg 5,5 kW three-phase four-pole squirrel cage electrical motor, and the alternator is a 5.5 kVA Mecc Alte spa three-phase alternator. Two accelerometers were used to measure the vibration signals on the monitored gearbox. The first accelerometer is the Wilcoxon ICP uni-axial accelerometer, which is mounted on top of the gearbox casing. The second accelerometer is a 100 mV/g PCB ICP tri-axial accelerometer which cannot be seen in the setup, it is mounted on the side of the gearbox casing.

In a helical gearbox system, the pinion and gear teeth are prone to local faults including root cracks, tooth wear, chipped tooth, and broken teeth because they experience high load due to harsh environmental conditions. For these reasons, a root crack on the gear tooth located in the monitored gearbox is created in our experiments. The gear has 37 teeth, and the pinion has 20 teeth, and thus the gear ratio of the helical gearbox is $37/20 = 1.85$. The gear before and after the fatigue experiment is shown by a cracked and broken tooth, which is illustrated in Fig. 6. An eight-channel OROS OR35 data acquisition system is used to acquire the vibration signal for further processing.

The rotational speed profile displayed in Fig. 7 in was measured using a Zebra-strip shaft encoder with 88 pulses per revolution and Optel Thevon optical switch. The vibration signals were collected under various loading conditions and rotating speeds. The sampling frequency Δ_f is 25.6 kHz, sampling length is almost 20 sec. A sampling frequency Δ_f of 51.2 kHz is used for the Optel Thevon optical switch to capture the shaft position accurately on the Zebra-strip shaft encoder. During the fatigue experiment, a total of 1400 files were collected. However, only 200 files ranging from files 1 to 1400 with equal spacing will be used to capture the damage signal from inception to completion of this experiment.

The rotational speed profile ranging between 13 to 18 rad/s is imposed on the motor to represent the time-varying operating conditions. This operating condition provides sufficient complexity to critically evaluate the performance of the proposed methods in diagnosing the gear fault with low-impact energy. The time-varying operating conditions are expected to cause both amplitude and phase modulation on the measured vibration signal. As a result, the measured vibration signal of the gear fault is often a mixture of the CNS1 signals, background noise, and CNS2 signals.

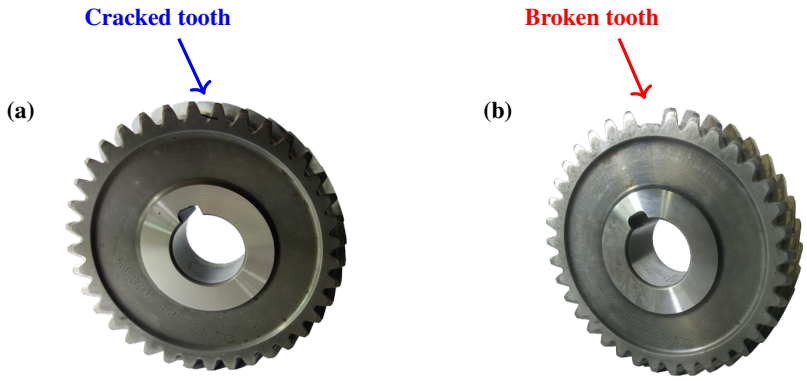

Figure 6: Helical gear in the C-AIM experimental test rig (a) gear with 50% cracked tooth representing incipient fault, and (b) gear with broken tooth representing matured fault [51].

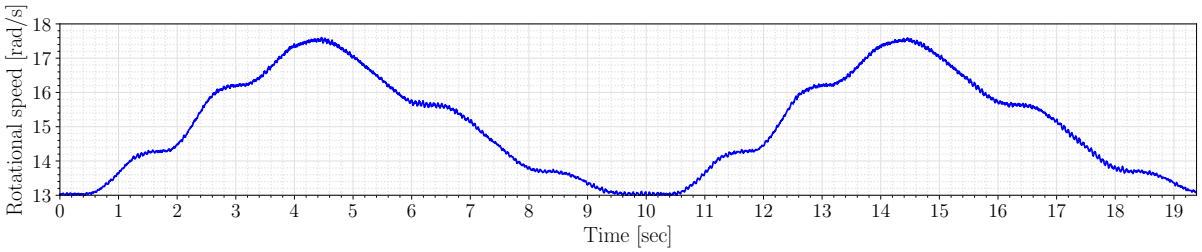

Figure 7: The rotational speed profile for C-AIM experimental test rig.

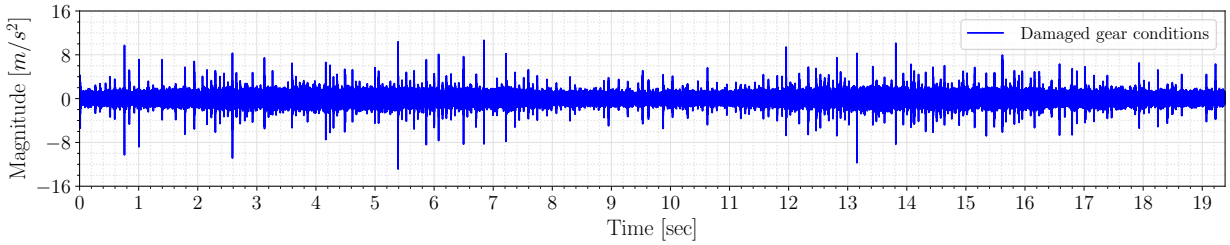

Figure 8: Acceleration signals acquired from the helical gearbox casing with damaged gear conditions.

The measured vibration signal illustrated in Fig. 8 represents the localised gear fault at an incipient stage respectively. Looking at the measured vibration signals, it is not possible to conclusively identify the localised gear fault. This vibration signal is heavily clouded by strong interference with substantially large magnitudes. This interference appears on both vibration signals with healthy gear conditions and damaged gear conditions. This impedes the application of many conventional signal-processing techniques. In the next section, we study the kinematics of the first-order cyclo-non-stationary signals (i.e. a deterministic part of CNS signal) which are known to mask the gear and bearing fault signatures of the gearbox system under non-stationary conditions.

5.2. The framework of SM-IPSgram in gear diagnostics

This section gives a comprehensive and systematic framework of the detailed applications of sparsity measures on the IPS representation. First, some important challenges related to harsh operating conditions are summarised to underline the need for a robust IFB identification method. Throughout this section, our attention will be confined to the case of a helical gear fault which is a challenge due to low-impact energy. In Section 5.2.1, we present the classical SA-IPS and the whitened SM-IPS. In Section 5.2.2, we present the mathematical computation for the whitened SM-IPS estimation of sparsity measures. In Section 5.2.3, the binary tree filter banks for classical SA-IPS and whitened SM-IPS are compared in terms of diagnostic capabilities.

5.2.1. The whitened synchronous median instantaneous power spectrum

The object of this section is to assess the performance of the classical SA-IPS and whitened SM-IPS which are the extension of the IPS within the *angle-time cyclostationary* (AT-CS) framework. The theory of AT-CS signal is recognised as an effective tool for machine condition monitoring under extreme conditions. This theory has emerged in the last decade as a novel approach for characterising CS2 signals. Many research efforts have been made using this theory which led to several technological breakthroughs. One major property of the CS2 signals is that they can be isolated from compound faults with ease, allowing the detection of weak faults hidden in high levels of stationary noise and deterministic components. For the sake of a juster comparison, the SA-IPS and whitened SM-IPS are computed and displayed in Fig. 9 with the aim of detecting the localised gear fault at an incipient stage.

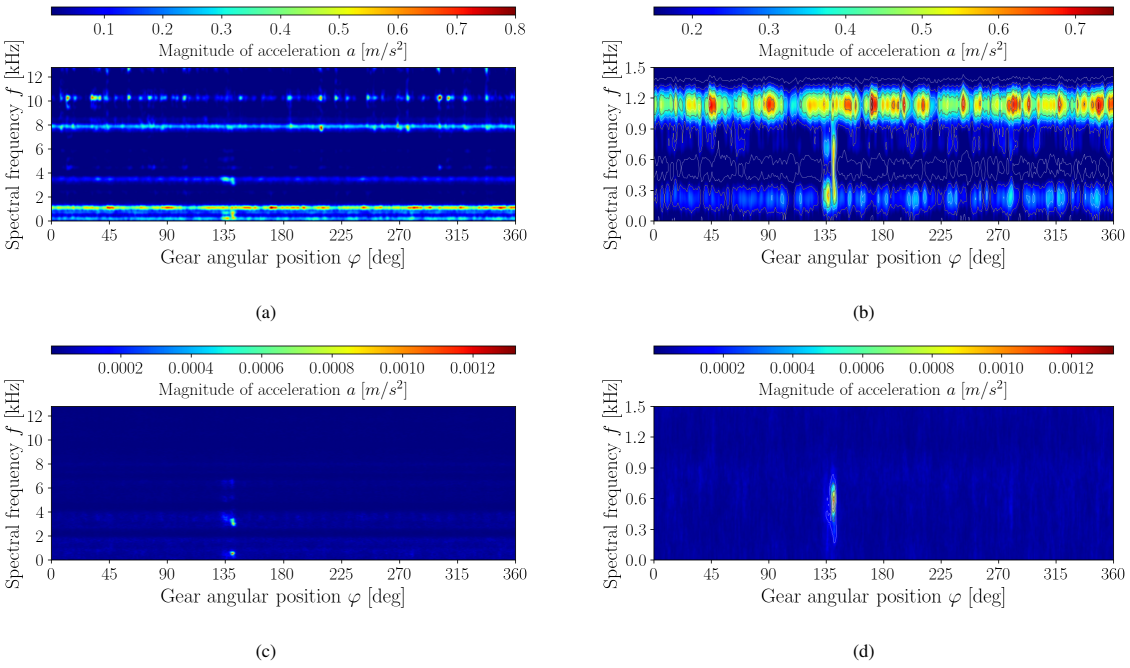

Figure 9: (a) averaged instantaneous power spectrum for raw signal, (b) zoomed spectra with strong deterministic gear components, (c) synchronous median instantaneous power spectrum for whitened signal, and (d) zoomed spectral with evidence of localised gear fault.

The SA-IPS (see Fig. 9(a)) covers a spectral frequency range of [0–12.8] kHz and an angular position of [0–360] deg. The location of the faulty tooth is at about 135 deg and is barely visible due to deterministic gear components and strong interference. The deterministic gear components appearing at spectral frequency range [0-1.5] kHz and 8 kHz cover the whole angular position axis. There exist several impacts that appear at about 10.4 kHz which resemble localised faults, space randomly over the angular position. These impulsive interferences are related to the interference on the bearing outer race. They merit attention, in view of their possible influence on the selected IFB. Consequently, it becomes apparent that the averaging in general is not resistant to outliers, and thus may lead to erroneous diagnostic conclusions because the localised gear fault remains undetected in this specific case. The

performance of the SA-IPS degrades significantly in the presence of strong interference and non-Gaussian noise and thus it cannot be expected to give more than a somewhat rough result. To separate this strong interference is a matter of great difficulty but of much importance to gear diagnostics.

In contrast, the localised gear fault is clearer and more visual on the whitened SM-IPS shown in Fig. 9(c). This approach provides an effective and reliable way of maintaining the original signal structure by suppressing background noise and interference. There exist two major IFBs at an angular position of 135 deg around the spectral frequency range of [0-1] kHz and [3-4] kHz. There are several minor IFBs in the spectral frequency range of [5-7] kHz. In practical application, many types of gear faults including fatigue cracks or spalls are localised and hence their angular position is very short as compared with the angular position for one complete revolution of the gear. These results are promising and strongly indicate that the information can be used to pave a binary tree using sparsity measures. In the next section, this representation will be used, together with the sparsity measures to obtain a filter banks decomposition. We also intend to show how many of the disadvantages of the sparsity measures can be overcome by the whitened SM-IPS and to indicate some of their useful properties in gear diagnostics.

5.2.2. The sparsity measures

It has been long known that the sparsity measures can identify IFB within reasonable computational times and therefore they have the potential to be used as a basis to develop the IFB identification method efficiently. In this section, the spectral kurtosis, Hoyer index, and the spectral log-mean-exp are considered. To allow a fair comparison of these sparsity measures in diagnosing the localised gear fault, we first need to define them in terms of the whitened SM-IPS. This will necessitate a slight modification of the definition of these sparsity measures. This modification we now wish to investigate this in order to give it a new meaning.

Spectral kurtosis: In the literature, spectral kurtosis has been considered by several authors from various perspectives and it is mostly used for STFT-based fast Kurtogram to locate the carrier/spectral frequencies of the repetitive transients in the vibration signal. The mathematical computation for the whitened SM-IPS estimation of the spectral kurtosis, $SK_\varepsilon(f, \Delta f)$, is given as:

$$SK_\varepsilon(f, \Delta f) = \frac{\left\langle \left| \varepsilon_x^\phi(\varphi; f, \Delta f) \right|^4 \right\rangle}{\left\langle \left| \varepsilon_x^\phi(\varphi; f, \Delta f) \right|^2 \right\rangle^2} - 2 \tag{11}$$

where $\varepsilon_x^\phi(\varphi; f, \Delta f)$ denote the whitened SM-IPS, f is the spectral frequency, $\Delta f = \Delta_f / N_w$ is the bandwidth or spectral frequency resolution calculated from sampling frequency Δ_f and the window length N_w, and a constant value of negative 2 make use of Fisher's definition (i.e. spectral kurtosis becomes zero for Gaussian noises) to normalise the spectral kurtosis when complex Gaussian noises are considered as an input to spectral kurtosis.

Spectral Hoyer index: In the literature on sparsity measures, the Hoyer index which satisfies at least five of six criteria that are necessary for the measurement of sparsity is the second-best sparsity measure after the Gini index and *pq-mean* [35]. However, as far as we know, there is no precise and unambiguous sparsity measure or blind indicator which may be termed the most accurate available in identifying the optimal filter band for demodulation. We shall revert to this point in Section 5.4.4. The mathematical computation for the whitened SM-IPS estimation of the spectral Hoyer index, $HI_\varepsilon(f, \Delta f)$, is given as:

$$HI_\varepsilon(f, \Delta f) = \left(\sqrt{L_\varphi} - \frac{\langle \varepsilon_x^\phi(\varphi; f, \Delta f) \rangle}{\sqrt{\langle \varepsilon_x^\phi(\varphi; f, \Delta f) \rangle^2}} \right) \Big/ \left(\sqrt{L_\varphi} - 1 \right) \tag{12}$$

where $\varepsilon_x^\phi(\varphi; f, \Delta f)$ denote the whitened SM-IPS, f is the spectral frequency, $\Delta f = \Delta_f / N_w$ is the bandwidth or spectral frequency resolution calculated from sampling frequency Δ_f and the window length N_w.

Spectral log-mean-exp: The full theoretical mathematical description of the spectral log-mean-exp is given in Section 3.3. This subsection present only the mathematics pertinent to our implementation. Hence, the mathematical computation for the whitened SM-IPS estimation of the spectral log-mean-exp, $LME_\varepsilon(f, \Delta f)$, is given as:

$$LME_\varepsilon(f, \Delta f) = \max \left\{ \frac{\varepsilon_x^\phi(\varphi; f, \Delta f)}{\langle \varepsilon_x^\phi(\varphi; f, \Delta f) \rangle} \right\} + \ln \left(\frac{1}{L_\varphi} \sum_{\varphi=0}^{L_\varphi - 1} \exp \left(\frac{\varepsilon_x^\phi(\varphi; f, \Delta f)}{\langle \varepsilon_x^\phi(\varphi; f, \Delta f) \rangle} - \max \left\{ \frac{\varepsilon_x^\phi(\varphi; f, \Delta f)}{\langle \varepsilon_x^\phi(\varphi; f, \Delta f) \rangle} \right\} \right) \right) \tag{13}$$

where $\varepsilon_x^\phi(\varphi; f, \Delta f)$ denote the whitened SM-IPS, f is the spectral frequency, $\Delta f = \Delta_f / N_w$ is the bandwidth or spectral frequency resolution calculated from sampling frequency Δ_f and the window length N_w.

5.2.3. SM-IPSgram for gear diagnostics

The author commences by considering a very simple approach, consisting of applying a blind indicator of the classical SA-IPS. It should be explained at the outset that we have concentrated attention on this particular problem solely because our interest is centered on gear diagnostics. The incipient gear fault is represented by measurement 6, with a continuous record of finite length $L_t = 496298$ points. The maximum window length for 1/2-binary tree filter banks can be calculated as $N_w = 2^{\lfloor \log_2(496298) \rfloor} = 2^{\lfloor 18.9208 \rfloor} = 2^{18}$, the sampling frequency Δ_f is 25.6 kHz. The smallest bandwidth is calculated as $f_{bw} = \Delta_f / N_w = 0.0976$ Hz. However, its value is very small to capture a fault and it adds computational costs as well. As a result, the maximum window length can be reduced to a smaller value. In this section, a window length of 2^{14} is used and this gives a bandwidth of $f_{bw} = \Delta_f / N_w = 1.5625$ Hz. The overlap fraction R of 0.75 with a Hanning window will be used for binary trees. Here, we aim to show the effect of the strong interferences on the performance of the 1/2-binary tree paved using a well-known sparsity measure on the SA-IPS before approaching the development of the SM-IPSgram.

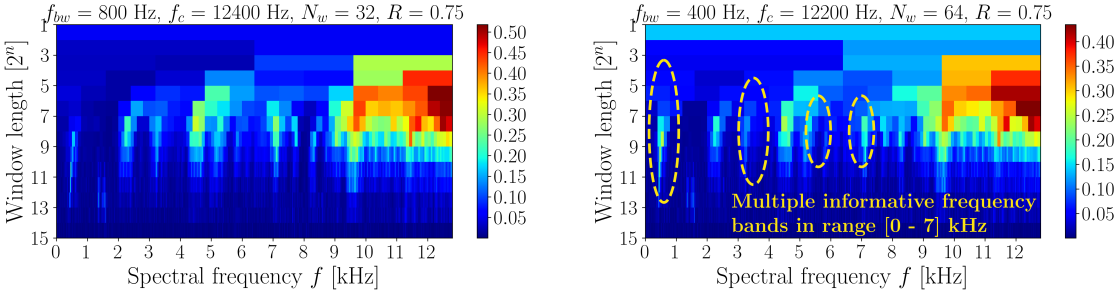

(a) (b)

Figure 10: 1/2-binary tree paved using Hoyer index on the (a) SA-IPS, and (b) whitened SA-IPS.

In the literature on sparsity measures [29], the Hoyer index is the second best after the Gini index. However, it has more nice properties and it has been verified to perform better than most sparsity measures. As a result, the Hoyer index is used as a sparsity measure on the SA-IPS to pave the 1/2-binary tree filter banks displayed in Figs. 10(a) and 10(b) to highlight the spectral frequency band $[f_{bw}, f_c]$ that carries rich diagnostic information about the impulsiveness of the enhanced modulating signal. The colours of the binary tree are correlated with the impulsiveness of the signal. Dark blue is for minimum impulsiveness and dark red is for maximum impulsiveness. Comparing the binary tree for raw and whitened SA-IPS, it is not possible to conclusively identify the IFB for localised gear fault. A simple visual inspection of spectral frequency in the yellow ellipses shows little information about the gear fault.

A glance at these binary tree filter banks shows that there is no systematic improvement. We can take this as our starting point to understand why we gave preference to whitened SM-IPS over the classical SA-IPS. Up to this point, the procedure was relatively simple except for the poor performance of the SA-IPS. This resulted in very feeble impulsiveness and consequently, long vibration signals must be acquired. It is futile to endeavour to obtain reliable guidance for selecting IFB from the blind indicators in the presence of non-Gaussian noise of strong interferences. The separation of strong interferences or non-Gaussian noise is unfortunately by no means easy. In order to make certain of extracting the spectral frequency of the localised gear fault only, it is essential to decompose the IPS at an angular period of interest using the synchronous median.

Illustrated in Fig. 11(a) is the 1/2-binary tree for raw SM-IPS. As expected, the method was not able to select the rich IFB because the spurious and deterministic components effectively obscure the gear fault. But, when comparing this method with previous results, the SM-IPS turns out to enhance the localised gear fault slightly because it attenuated high impulsiveness on the spectral frequency range [10, 12.8] kHz. The reason behind this is that the SM is effective in attenuating strong interferences and non-Gaussian noise. It is evident that when the SM-IPS is used, the principal difficulty relates to deterministic gear components, and that the impulsiveness related to strong interference became infinitesimally small. This may be taken as very strong evidence that the performance of the SM-IPS is in no way impaired by the presence of strong interferences in comparison to the SA-IPS. A higher degree of accuracy of the selected IFB might, therefore, reasonably be expected. However, the SM cannot attenuate the deterministic gear components. This approach performs sub-optimally and cannot be expected to give more than a somewhat rough result.

At most, the spurious harmonics due to deterministic gear components were conceded to be a possible cause for obscuring the IFBs of the localised gear fault. It should be mentioned that although the utmost care was taken to remove the strong interference with the SM-IPS, the deterministic gear components still present obscurity in our analysis. It is necessary to whiten the SM-IPS very carefully if the utmost degree of accuracy is desired. Hence, the 1/2-binary tree paved using the Hoyer index on the whitened SM-IPS is computed and displayed in Fig. 11(b). This approach produces the filter banks decomposition to accentuate only the carrier/spectral frequency of the localised gear fault under strong interferences. As a result, this filter banks decomposition is named the SM-IPSgram. The novelty of this method lies in the fact that it can be used for identifying IFB and a weighting function. The

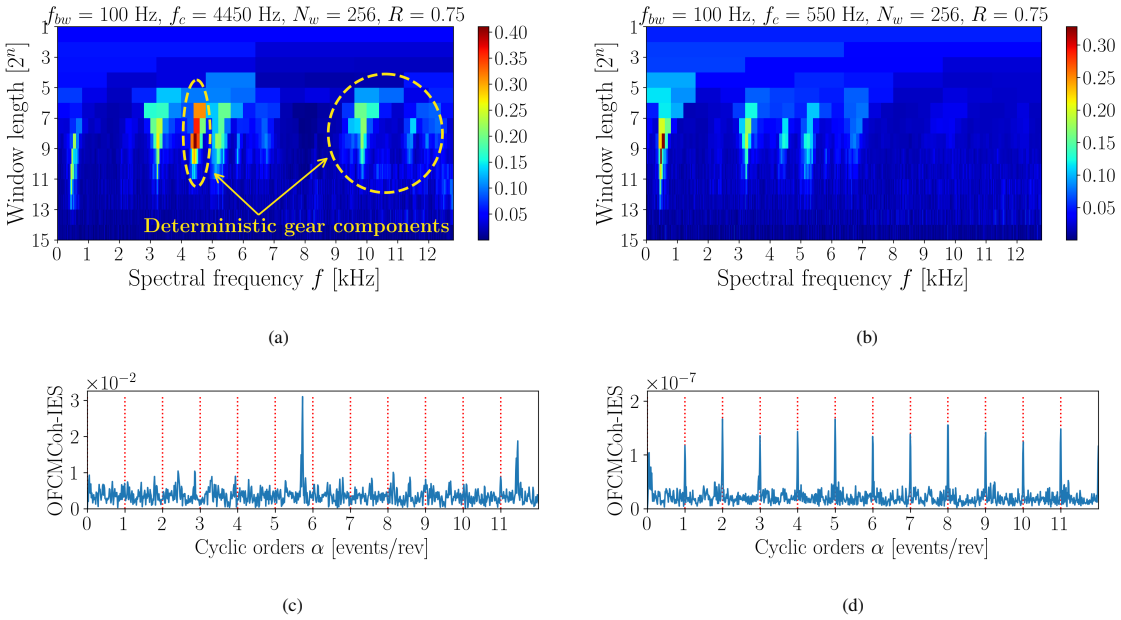

Figure 11: SM-IPSgram paved using the Hoyer index on (a) SM-IPS, (b) whitened SM-IPS, (c) WES of the frequency bands selected by the SM-IPSgram paved on the SM-IPS, and (d) WES of the frequency bands selected by the SM-IPSgram paved on the whitened SM-IPS.

SM-IPSgram before and after applying pre-whitening bear little resemblance to one another, the only peak common to both being at the spectral frequency in the range [3-4] kHz, unless we include the peak which appears at a lower spectral frequency in the range [0-1] kHz. The SM-IPSgram can identify the IFB with the requisite accuracy, for the vibration signal with strong interferences. There is thus nothing surprising in the fact that the whitened SM-IPS can attenuate most of the phenomena asynchronous to the desired angular period $\phi = \alpha_{fault}^{-1}$.

To evaluate the performance of the methods in identifying rich IFB related to the fault, the *improved envelope spectrum* (IES) of the *order-frequency cyclic modulation coherence* (OFCMCoh) are computed and displayed in Figs. 11(c) and 11(d). It is worth recalling that the spectral frequency f contains information related to machine dynamics, while the cyclic orders contain rich diagnostic information related to machine kinematics. The purpose of the OFCMCoh-IES is to utilise this kinematic information at a specific frequency band to detect the presence of a defect based on the cyclic orders α. The OFCMCoh-IES computed from the IFB on the 1/2-binary tree of the raw SM-IPS (see Fig. 11(c)) clearly shows that it failed to identify the IFB due to deterministic gear components. In contrast, the OFCMCoh-IES computed from the IFB on the SM-IPSgram (see Fig. 11(d)) was able to capture rich diagnostic information. This approach can provide effective and reliable IFB.

5.3. The fast Kurtogram and the ICS2gram

In the earlier sections, the proposed SM-IPSgram has made it easy to carry out the estimation of the IFB and it forms a very valuable indication of the presence of the localised gear fault. However, in order to assess the practical accuracy of such a method, it is necessary to compare its results with those of more well-known analyses. In this section, the 1/3-binary tree which has higher resolution as compared to the 1/2-binary tree will be used to identify the optimal demodulation band. Moreover, the intrinsic properties of the SM-IPSgram are pointed out and systematically compared to the fast Kurtogram and the ICS2gram. The former is a blind method that selects a band with maximum impulsiveness, whilst the latter is a targeted method that selects a band with maximum ICS2 content.

Illustrated in Figs. 12(a) and 12(b) are the SM-IPSgram estimation of the spectral log-mean-exp, and the fast Kurtogram respectively. Both methods identified the IFB with maximum impulsiveness, but from diametrically opposite points of view. In this case of the localised gear fault of the helical gearbox, the load is shared across a large face width of a tooth, and this makes the IFB identification using the fast Kurtogram difficult since the changes in vibration are smaller as compared to strong interference. As a result, the fast Kurtogram gave a misleading IFB of $\{f_{bw}; f_c\} = \{1067 \text{ Hz}; 12267 \text{ Hz}\}$, which is almost similar to that of the sparsity measure on the SA-IPS represented in a 1/2-binary tree (see Fig. 10). On the other hand, it is seen that the SM-IPSgram estimation of the spectral log-mean-exp is insensitive to the strong interferences and clearly reveals multiple IFBs in the spectral frequency range [0-7] kHz. In particular, the optimal demodulation band of $\{f_{bw}; f_c\} = \{100 \text{ Hz}; 550 \text{ Hz}\}$, is associated with maximum impulsiveness produced by the localised gear fault.

The fast Kurtogram has become famous because it is the first successful attempt to introduce a little more scientific precision into the treatment of problems that involve automatic IFB identification by using spectral kurtosis. However, this classical approach is

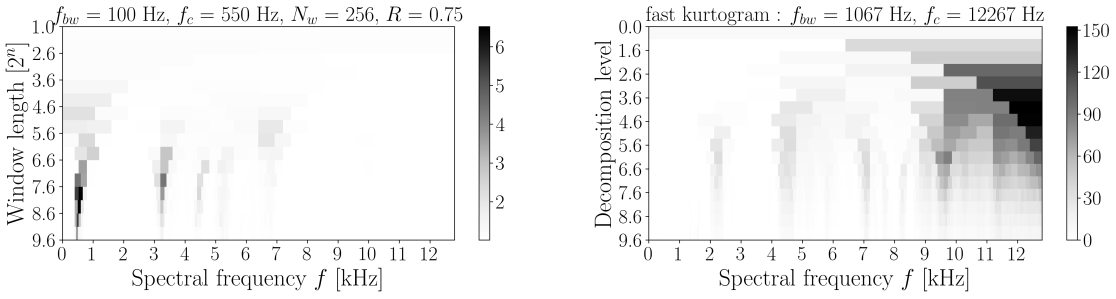

(a) (b)

Figure 12: Localised gear fault: (a) SM-IPSgram estimation of the spectral log-mean-exp, and (b) fast Kurtogram.

open to criticism in light of modern standards of accuracy and robustness. It is doubtful whether a high degree of accuracy can be attained by this fast Kurtogram since the blind methods usually perform sub-optimally as compared to targeted methods. In general, the discordance between the IFB on the SM-IPSgram and fast Kurtogram is very significant, and this demonstrates the superiority of the former over the latter. We must conclude that the blind method such as the fast Kurtogram is quite insufficient for determining the reliable IFB in the presence of strong interferences.

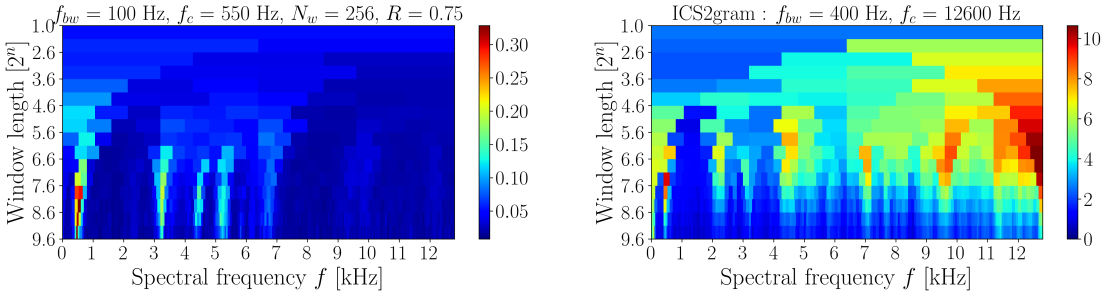

(a) (b)

Figure 13: Localised gear fault: (a) SM-IPSgram estimation of the spectral Hoyer index, and (b) ICS2gram.

The results obtained are quite remarkable, as seen by comparing the SM-IPSgram and the ICS2gram in Figs. 13(a) and 13(b) respectively. It has become evident that there are definite limitations in the ICS2gram, like all methods of analysis, which greatly restrict its usefulness in gear diagnostics under strong interferences. In this specific case, the ICS2gram gave what purported to be optimal filter band, $\{f_{bw}; f_c\} = \{400 \text{ Hz}; 12600 \text{ Hz}\}$, that contained the localised gear fault. Had it been possible to remove the strong interference from the squared envelope spectrum, the IFB identification of the localised gear fault would not have been different from that of the SM-IPSgram. Generally, the fast Kurtogram and this approach performed the same when comparing the IFB. However, the ICS2gram can potentially reveal weak gear damage more effectively than the fast Kurtogram. We conclude with considerable assurance that the SM-IPSgram is the most robust IFB identification method that can be used in gear diagnostics in the presence of non-Gaussian noise and strong interference. The proposed SM-IPSgram, which performs comparatively better than other reported methods in literature guarantees reliable performance in gear diagnostics.

5.4. SM-IPSgram estimation of the sparsity measures

To further lay a clear foundation for the concept of spectral log-mean-exp, this section presents the SM-IPSgram estimation of the sparsity measures and discusses the similarities and differences of the filter banks decomposition when being implemented using 1/2 and 1/3-binary trees. Each sparsity measure is first outlined and its properties concerning the detection of the localised gear faults are shortly examined. In practice, the most frequently discussed facets of IFB identification methods include the binary tree filter banks which is directly related to the resolution. Hence, it was considered essential to present both the 1/2 and 1/3-binary tree in a sufficiently elementary manner so that it might become apparent why we choose the latter over the former.

5.4.1. The spectral kurtosis

The notion of binary tree filter banks is a well-recognised and useful concept in signal processing for efficient accurate automatic identification of the IFB. The 1/2-binary tree and 1/3-binary tree are used frequently and variously in paving the binary tree filter

banks. Some researchers employ them interchangeably; others use them consistently in a specific manner. The question naturally arises as to how these binary trees should be used in practice. This section will provide in sufficient detail the various approaches to implementing binary tree filter banks. Hence, the 1/2 and 1/3-binary trees for SM-IPSgram estimation of the spectral kurtosis are presented in Fig. 14, respectively.

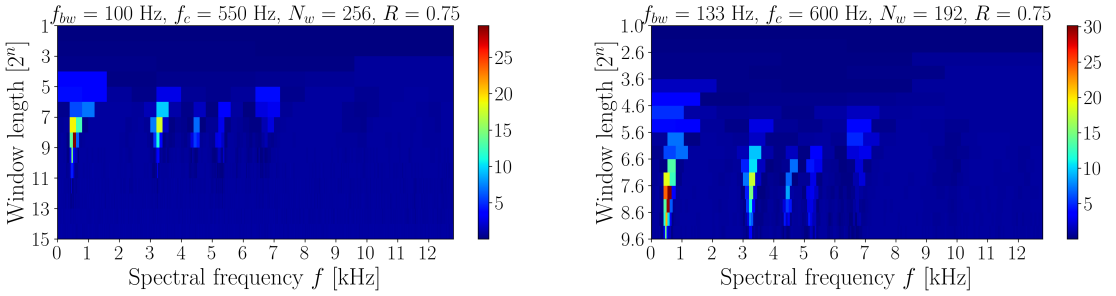

(a) (b)

Figure 14: The SM-IPSgram estimation of the spectral kurtosis: (a) 1/2-binary tree, and (b) 1/3-binary tree.

As expected, the SM-IPSgram estimation of the spectral kurtosis produced a filter banks decomposition to accentuate only the spectral frequencies of the localised gear fault. The whitened SM-IPS in general makes it possible to remove any periodic events not exactly synchronous with the localised gear fault and to attenuate strong interferences and vibration sources other than the considered gear fault. In this case, the maximum window length of $N_w = 2^9$ is used on the 1/3-binary tree. Based on the results of the 1/2-binary tree (see Fig. 14(a)), the range of window lengths on the 1/3-binary tree seems intuitively reasonable: a smaller window length N_w less than or equal to 2^4 may not provide enough spectral frequency resolution to capture narrowband localised gear faults, while a higher window length N_w greater than or equal to 2^{11} not provide enough impulsiveness on the modulating signals. Hence, in general, it will be wasteful to demand more frequency resolution than we actually need. This maximum window length secures a reasonable impulsivity of the modulating signals. In this specific case, the OFCMCoh-IES for both representations look similar to the results presented in Fig. 11(d).

Generally speaking, the spectral kurtosis enjoyed many useful properties including reliable IFB identification in the presence of strong interferences because the SM-IPSgram merges the benefits provided by whitened SM-IPS with the benefits provided by the spectral kurtosis. However, it has been long known that spectral kurtosis loses this superiority when interference exists in the measured vibration signal. This has been demonstrated using the fast Kurtogram which performed sub-optimally in diagnosing the localised gear fault. This obviously adheres to our intuition since the spectral kurtosis only measures impulsiveness, and thus it cannot distinguish between non-Gaussian noise, interferences, and repetitive transients which are impulsive in nature.

5.4.2. The spectral Hoyer index

In the previous subsection, the SM-IPSgram estimation of the spectral kurtosis has been demonstrated to provide consistently reliable guidance for identifying optimal demodulation bands. This section considers the case of SM-IPSgram estimation of the spectral Hoyer index. Hence, the 1/2 and 1/3-binary trees are presented in Fig. 15. The performance of the SM-IPSgram estimation of the spectral Hoyer index is almost similar to that of the spectral kurtosis. Nevertheless, the concept of the SM-IPSgram enables a more detailed analysis of the spectral frequencies of the localised gear fault and leads to a physically meaningful interpretation of underlying phenomena in the presence of strong interferences.

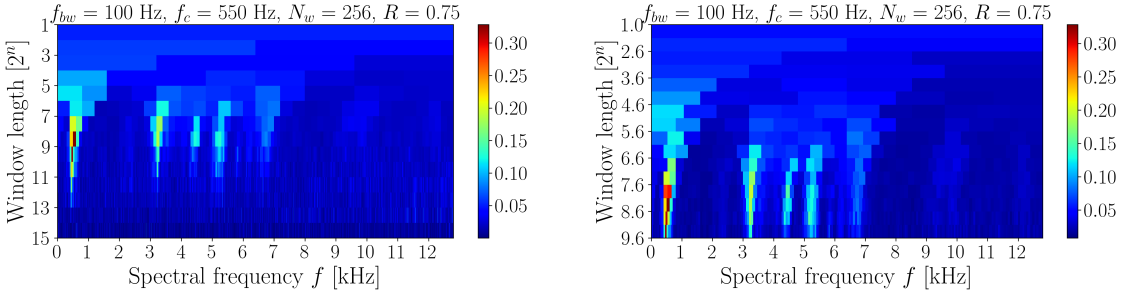

(a) (b)

Figure 15: The SM-IPSgram estimation of the spectral Hoyer index: (a) 1/2-binary tree, and (b) 1/3-binary tree.

All these sparsity measures have certain peculiar features in common, which are mainly rooted in the fact that they make use of different statistical features. It is clear that we cannot decide which method of analysis is appropriate before we have investigated the performance of these sparsity measures under a variety of operating conditions. As will appear in a Section 5.4.4, the performance of the sparsity measures is not necessarily the same on different measurement numbers, but the IFB is almost the same for most occasions.

This approach has the very great advantage that it attenuates both interferences and deterministic gear components and that the sparsity measures are simple. Even though the 1/3-binary tree is probably preferable to the 1/2-binary tree, for this specific case, it does not make any difference whether one used the 1/2-binary tree or a 1/3-binary tree since the identified IFB is exactly the same. For extreme cases where the N_w is very large (e.g. $N_w \geq 2^{12}$) the value selected by blind indicators tends to zero because of the Central Limit Theorem. On contrary, the smaller N_w (e.g. $N_w \leq 2^4$) leads to significantly large bandwidth, $f_{bw} = \Delta_f / N_w$ which may not allow the blind indicators to detect the faults with narrowband.

5.4.3. The spectral log-mean-exp

In this subsection, the performance of the proposed spectral log-mean-exp is assessed and its intrinsic properties are pointed out and compared to the spectral kurtosis and the Hoyer index. The binary tree filter banks for spectral log-mean-exp as a sparsity measure are presented in Fig. 16. Before considering the main results of the intercomparison of the three sparsity measures considered, it will be convenient to refer to some incidental facts which were disclosed in the preceding sections. A question of interest is whether any sensible systematic difference exists between the spectral kurtosis and log-mean-exp. Looking at different levels of the window length $[2^n]$, it is apparent that there is no perceptible difference between the proposed log-mean-exp and the spectral kurtosis other than the identified IFB on the 1/3-binary tree.

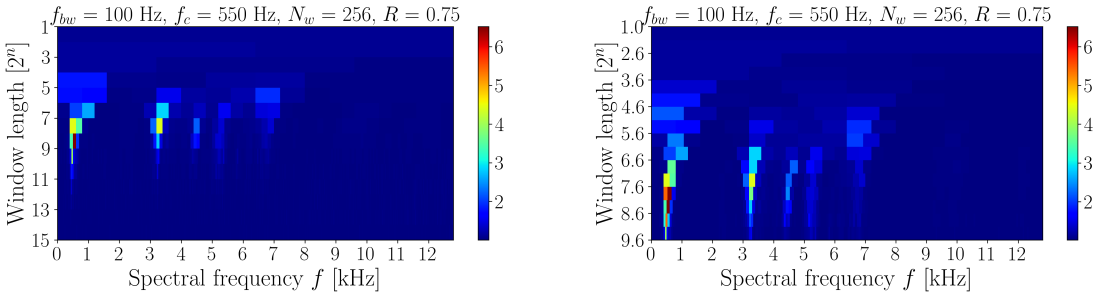

(a) (b)

Figure 16: The SM-IPSgram estimation of the spectral log-mean-exp: (a) 1/2-binary tree, and (b) 1/3-binary tree.

Therefore, it seemed desirable to make a more exhaustive investigation of the IFB of various these sparsity measures under different measurement numbers, with a view to obtaining the filter bands and ascertaining if the spectral kurtosis and log-mean-exp are interrelated. In general, we wish for an IFB identification method to extract the spectral frequencies of the defect. This approach seems to be appropriate for gear diagnostics under harsh operating conditions. To conclude, the spectral log-mean-exp is simple and reliable, and its performance is comparable to that of the classical sparsity measures. The SM-IPSgram of the sparsity measures seems quite effective in detecting developing localised gear faults. The technique excels in accentuating the spectral frequencies of the faults in the presence of strong interferences.

5.4.4. Comparison between three sparsity measures

The preceding results did not absolutely show any perceptible systematic difference in identifying IFB. Thus, we cannot reach any conclusion about the performance of the proposed log-mean-exp as compared to other sparsity measures. To diminish the risk of arriving at erroneous conclusions the performance of the sparsity measures is accessed for different measurement numbers. The object of the present investigation has been to obtain quantitative about the performance of the sparsity measures, and more especially to ascertain the centre frequencies f_c and the magnitude of the bandwidths f_{bw}. Hence, the identified IFB, $[f_{bw}; f_c]$, of the SM-IPSgram estimation of the three sparsity measures represented in a 1/3-binary tree for different measurement numbers are computed and displayed in Fig. 17. It is noticed that the centre frequency f_c for three sparsity measures is all much the same, the most noticeable difference being that they are sensitive to impulsiveness in different spectral frequencies of the localised gear fault. One of the most curious facts about blind indicators is that they perform differently in identifying impulsiveness of the enhanced modulating signals. The IFBs on the spectral log-mean-exp and spectral kurtosis are by no means *sui generis*, and a remarkable instance has been observed in the case of their bandwidths. All the sparsity measures give the remarkably close agreement of the IFB for localised gear fault.

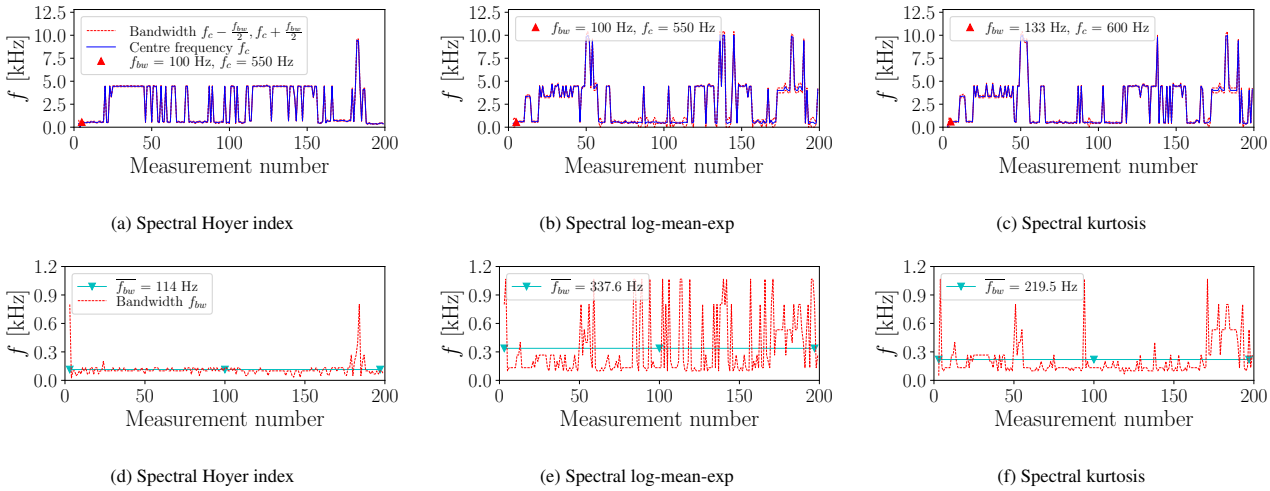

(a) Spectral Hoyer index (b) Spectral log-mean-exp (c) Spectral kurtosis

(d) Spectral Hoyer index (e) Spectral log-mean-exp (f) Spectral kurtosis

Figure 17: The IFB of the SM-IPSgram estimation of the three sparsity measures represented in a 1/3-binary tree for different measurement numbers.

The bandwidth f_{bw} varies very little throughout a measurement number, such that throughout this range the bandwidth will be very nearly constant. Hence, if we draw a graph to represent the mean bandwidth $\overline{f_{bw}}$, we get very approximately a straight line that represents the bandwidth throughout the measurement number accurately. It is clear that the SM-IPSgram estimation of the spectral Hoyer index (see Fig. 17(d)) has the merit of giving nearly constant bandwidth for various measurement numbers. The fact that this results of the bandwidth f_{bw} shows that there is no striking resemblance between the spectral log-mean-exp and spectral kurtosis (see Figs. 17(e) and 17(f)), except for a measurement number 1 up to 50, while the centre frequencies were almost the same for almost all the measurement number, was at first very puzzling; but it began to dawn on us that the exponential function of the spectral log-mean-exp is able to identify IFB with much more impulsiveness on the squared envelope of the complex envelope.

As anticipated in previous subsections, the performance of the spectral log-mean-exp and kurtosis are nearly the same for the considered cases. Hence, it would be exceedingly interesting to investigate whether there exists any mathematical relation between the log-mean-exp and the spectral kurtosis. We believe that the accuracy of the identified IFB for different measurement numbers is sufficient to establish the conclusion that it is intended to draw from them. In general, the centre frequency f_c was roughly concordant throughout the measurement number. However, the proposed spectral log-mean-exp ensures a much broader bandwidth than the Hoyer index and spectral kurtosis, which is believed to provide consistently reliable guidance for selecting a rich filter band. In practice, a narrow bandwidth may lead to a poor filter band that excludes most of the diagnostic information. On the other hand, a broader bandwidth than necessary may lead to high noise content.

The sparsity measures are indeed the core impetus for developing the IFB identification method, thus facilitating effective fault diagnostics while reducing computational costs. As a result, the SM-IPSgram estimation of the sparsity measures is seen as promising IFB to tackle non-Gaussian noise and strong interferences, their success of them is very dependent on sparsity measures and prior knowledge of the fault period. The SM-IPSgram is found to offer distinctive features in the presence of many types of background noises. Another key finding is that the full spectral frequency corresponding to maximum impulsiveness offers a better weighting function that is rich with diagnostic information.

5.5. Weighting function based on the SM-IPSgram

Some progress has been made to develop a weighting function or a *combined improved envelope spectrum* (CIES) from the IFB identification method, and in this connection, we may mention the work of Mauricio and Gryllias in Ref. [21], who established a general method for identifying a multiband envelope spectra extraction. However, cyclo-stationary interferences have been the chief obstacle to the progress of the CIES approach. Even though this matter appears very simple, it has been found in practice to be fraught with very serious difficulties which have taken a long time to overcome. As a result, comparatively few investigations have been carried out to use the IFB identification methods for extracting multiple IFBs.

In this section, we will briefly discuss the weighting functions based on the SM-IPSgram to show their applicability for combining multiple IFBs and compare their performance with the existing results. By using a full spectral frequency corresponding to maximum impulsiveness on the SM-IPSgram (e.g. $\{N_w; R\} = \{256; 0.75\}$ for SM-IPSgram estimation of the spectral log-mean-exp), it appeared possible to throw a little more light upon the problem of the weighting function or CIES of the localised gear fault under strong interferences. Hence, the weighting functions to regulate the contribution of each spectral frequency band for the SM-IPSgram estimation of the three sparsity measures is presented in Fig. 18. This approach gives a systematic and consistent means of designing a weighting function in a manner that is both new and precise.

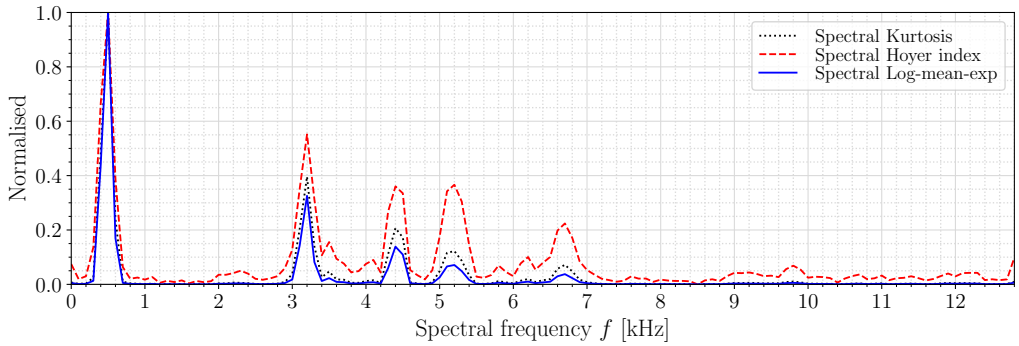

Figure 18: The weighting function estimation of the three sparsity measures, that is calculated from the whitened SM-IPS using $\{N_w; R\} = \{256; 0.75\}$ which correspond to maximum impulsiveness on the SM-IPSgram.

From the preceding results, it can be seen that the spectral Hoyer index may lead to high noise content. On the other hand, the spectral kurtosis and log-mean-exp may provide reliable weighting functions that attenuate noise content, especially on the higher spectral frequencies in the range of [7-12.8] kHz. However, when considering these pieces of information closely, we see immediately that the spectral log-mean-exp performs effectively in regulating the contribution of each spectral frequency band. It is believed that certain formal advantages accrue from the present approach, particularly with respect to robustness to strong interference. The weighting function can be multiplied with the OFCMCoh. The CIES estimators are computed by averaging the modified OFCMCoh over the entire spectral frequency axis. Nevertheless, this approach is beyond the scope of this paper.

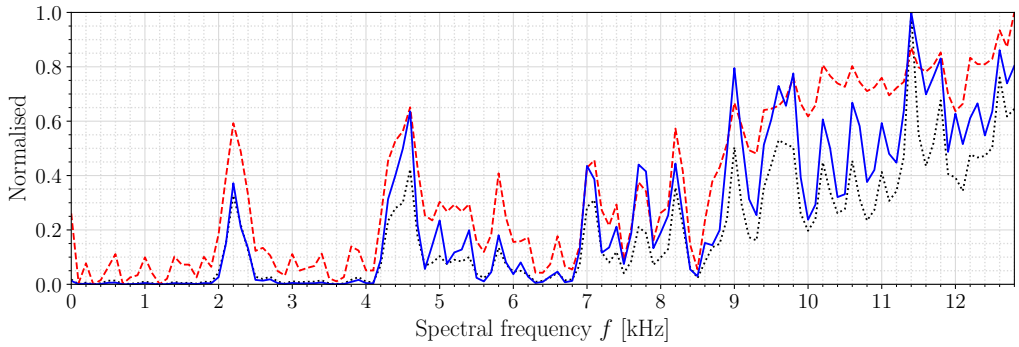

Figure 19: The weighting function estimation of the three sparsity measures, that is calculated from the whitened STFT using $\{N_w; R\} = \{256; 0.75\}$: (i) Spectral Kurtosis (black dotted line), (ii) Spectral Hoyer index (red dashed line), and (iii) Spectral Log-mean-exp (blue continuous line).

To exemplify the benefit of the whitened SM-IPSgram over the STFT, Fig. 19 shows the weighting function estimation of the three sparsity measures which were calculated from the STFT. This approach which has long been used to compute the spectral kurtosis [9, 10], provides a means of designing the weighting functions to regulate the contribution of each spectral frequency band. However, it is apparent that the strong interference impedes the application of the sparsity measures, and thus they cannot be expected to give more than a somewhat rough IFB of the localised gear fault. In this way, the proposed weighting function can be considered as a potential benefit, for the fact that it is sensitive to localised gear fault, and thus possesses advantages over this classical approach.

6. Numerical investigations

In this section, numerical results are presented in order to demonstrate the performance of the SM-IPSgram when it is exploited in diagnosing gear faults under harsh operating conditions. The phenomenological gearbox model will be used to represent the distributed gear fault under harsh operating conditions (i.e. in the presence of strong interferences, Gaussian and non-Gaussian noise). Emphasis is placed on a description of how the SM-IPSgram is robust to harsh operating conditions, and two examples are included to corroborate its effectiveness. At the end of this section, we demonstrate the superiority of the SM-IPSgram in identifying rich IFB of the distributed gear fault over a competing method, namely the ICS2gram.

6.1. Phenomenological gearbox model

The phenomenological gearbox model developed and proposed by Abboud *et al.* [52] will be used in this section to evaluate the performance of the proposed methods in a controlled environment. This model approximates the dynamic and kinematic behaviour of a faulty gearbox (i.e. gear and bearing faults). The results obtained from such a model are still consistent with real applications, while it is computationally efficient to calculate. The model parameters and equations as described by Schmidt *et al.* [53] will be used. The synthetic vibration signal from the gearbox model consists of four components:

$$x_{gb}(t) = x_{dg}(t) + x_{rg}(t) + x_b(t) + x_n(t) \tag{14}$$

where $x_{gb}(t)$ is the time waveform of a synthetic gearbox signal, $x_{dg}(t)$ is the deterministic gear component, $x_{rg}(t)$ is the random gear components, $x_b(t)$ is the bearing component and $x_n(t)$ is the background noise. The source signal is affected by transmission from the excitation source to the sensor. As a result, $x_{dg}(t)$, $x_{rg}(t)$, and $x_b(t)$ can be decomposed into a source signal and transmission path as follows:

$$x_{dg}(t) = h_{dg}(t) \otimes q_{dg}(t) \tag{15}$$

$$x_{rg}(t) = h_{rg}(t) \otimes q_{rg}(t) \tag{16}$$

$$x_b(t) = h_b(t) \otimes q_b(t) \tag{17}$$

where $h_{dg}(t)$, $h_{rg}(t)$, and $h_b(t)$ are the impulse response function that represents the transmission path from the excitation to the sensor. The convolution operator is denoted as $\otimes$ and the source signal of the deterministic gear, random gear, and bearing are presented as $q_{dg}(t)$, $q_{rg}(t)$ and $q_b(t)$ respectively. The general expression of the impulse response function of single-degree-of-freedom can be written as:

$$h_i(t) = e^{-\zeta_i 2\pi f_{n,i} t} \cdot \sin\left(2\pi f_{n,i} t \sqrt{1-\zeta^2}\right) \tag{18}$$

where $h_i(t)$ the impulse response function of component i, ζ_i represent the damping ratio, and $f_{n,i}$ represent the natural frequency.

$$q_{dg}(t) = M_{dg}(w_r(t)) \cdot \sum_{k=1}^{N_{dg}} A_{dg}^{(k)} \cdot \cos\left(k \cdot N_{t,g} \cdot \int_0^t w_r(\tau) d\tau + \phi_{dg}^{(k)}\right) \tag{19}$$

$$q_{rg}(t) = M_{rg}(w_r(t)) \cdot \varepsilon_{rg}(t) \cdot \sum_{k=1}^{N_{rg}} A_{rg}^{(k)} \cdot \cos\left(k \cdot \int_0^t w_r(\tau) d\tau + \phi_{rg}^{(k)}\right) \tag{20}$$

where $\int_0^t w_r(\tau) d\tau$ represents an angular position of the reference shaft rotating with the angular frequency w_r. $M_{dg}(w_r(t))$ and $M_{rg}(w_r(t))$ are monotonic functions simulating the dependence of the amplitude of the signal on the rotational speed. N_{dg} and N_{rg} are the number of gear mesh and random components respectively. $A_{dg}^{(k)}$ and $A_{rg}^{(k)}$ are the amplitudes. $N_{t,g}$ is the number of gear teeth. $\phi_{dg}^{(k)}$ and $\phi_{rg}^{(k)}$ are the phase. The general expression of the monotonic function $M_i(w_r(t))$ has the following form:

$$M_i(w_r(t)) = a \cdot w_r(t) + b \tag{21}$$

The main difference between Eq. (19) into (20), is that they contain an additional component which is $N_{t,g}$ and $\varepsilon_{rg}(t)$ respectively. The random component $\varepsilon_{rg}(t)$, can be expressed as a Gaussian distribution with zero mean and constant variance as:

$$\varepsilon_{rg}(t) \sim \mathcal{N}(0, \sigma_{rg}^2) \tag{22}$$

The surrounding or background noise component is written as:

$$x_n(t) = \varepsilon_n(t) \cdot M_n(w_r(t)) \tag{23}$$

with M_n being the monotonic function of w_r, and $\varepsilon_n(t)$ being the Gaussian distribution with zero mean and constant variance and has the following form:

$$\varepsilon_n(t) \sim \mathcal{N}(0, \sigma_n^2) \tag{24}$$

The last component is the outer race bearing damage which is simulated as a train of Dirac functions

$$q_b(t) = F_{dam} \cdot F_{const} \cdot M_b(t) \cdot \sum_{i=1}^{N_\mathcal{T}} \delta(t - \mathcal{T}_i) \tag{25}$$

The bearing slip is introduced by adding Gaussian noise with zero mean and a standard deviation of 0.1 to the expected impact angles. In order to simulate the gearbox with damaged bearing, $q_b(t) > 0$ is used. The signal-to-noise ratio (SNR) is defined as:

$$\text{SNR} = 10 \cdot \log_{10}\left(\frac{\sigma_b^2}{\sigma_n^2}\right) \tag{26}$$

Where σ_n^2 is the variance of additive noise and σ_b^2 is the observed signal. In the next section, the theoretical background of the alpha-stable distribution is introduced. This distribution will be used for the phenomenological gearbox model to represent the Gaussian and non-Gaussian noise to perform the sensitivity analysis of the proposed methods. The rotating speed profiles of the phenomenological gearbox model and their corresponding equations are shown in Section 6.1.1 (see Fig. 20).

6.1.1. Rotational speed profiles

In this section, the rotational speed profiles of the phenomenological gearbox model are presented. One of the aims of this paper was to perform fault diagnostics in the presence of time-varying operating conditions. Hence, the phenomenological gearbox model will be used throughout this section to represent the distributed gear fault under time-varying operating conditions. The model parameters and equations of the phenomenological gearbox model have four rotational speed profiles given as:

$$w_{r,1} = 2\pi \cdot (1.3t + 7) \tag{27}$$

$$w_{r,2} = 2\pi \cdot (5\sin(0.4\pi t) - 20 \cdot (0.1t - 0.5)^2 + 15) \tag{28}$$

$$w_{r,3} = 2\pi \cdot (6.5\cos(0.2\pi t) + 13.5) \tag{29}$$

$$w_{r,4} = 2\pi \cdot (6.5\sin(0.2\pi t) + 13.5) \tag{30}$$

The four rotating speed profiles are mathematically represented by $w_{r,1}$, $w_{r,2}$, $w_{r,3}$, and $w_{r,4}$. The speed profile 2, $w_{r,2}$ will be used in this section to represent the time-varying operating conditions for pseudo-CNS signals such as bearing outer race fault.

Illustrated in Fig. 20 is the rotational speed profile for the phenomenological gearbox model. Looking at the results, we can see the time-varying operating conditions which cause both amplitude and phase modulation on the measured vibration. In practice, the time-varying operating conditions are caused by many types of rotating machinery including wind turbines, making fault diagnostics of gears and bearings challenging.

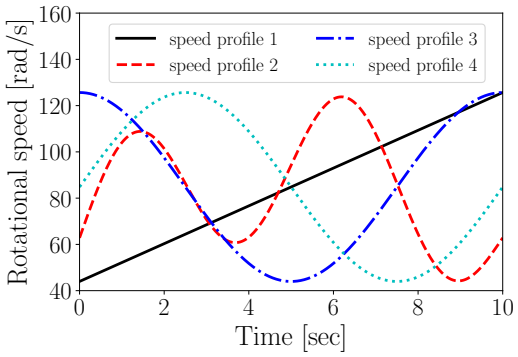

Figure 20: The rotational speed profiles for phenomenological gearbox model.

6.2. *Comparison between the SM-IPSgram and the ICS2gram*

In real-world applications, the measured vibration signal from a rotating machinery such as a gearbox is almost always interfered with by background noise including meshing gears, electronic noise, random noise, shafts misalignment, cyclo-stationary interferences from near mechanical components, and other parts. The combination of these signals reduces the *signal-to-noise ratio* (SNR). Hence, the detection of rotating machinery faults in the early stage is very difficult. Early detection of faults such as distributed gear faults is essential for the prevention of sudden tooth breakage which can lead to gear failure. Therefore, it is very important to extract useful features from the noise-contaminated mechanical signals.

In this section, the phenomenological gearbox model will be used to represent harsh operating conditions. This model is capable of describing the fundamental mechanisms and dynamics of gear vibrations in a controlled environment. To accurately model the distributed gear fault of the acceleration signals acquired from the gearbox casing, all of the potential vibration sources are taken into consideration in the synthesised signal of the phenomenological gearbox model. This includes the deterministic gear components, cyclostationary interferences, and Gaussian and non-Gaussian noises. The combined synthetic signals with the low-energy distributed gear fault are displayed in Fig. 21.

Four criteria have been selected to evaluate the merits of the proposed methods for the purpose of gear diagnosis in the presence of harsh operating conditions. This includes robustness against rapid speed fluctuation, interferences, Gaussian, and non-Gaussian noise. The amplitude modulations in the vibration signals were removed using NAMVOC [48]. The robustness against rapid speed fluctuation is evaluated using time-varying operating conditions which introduces amplitude and phase modulation in a vibration signal. The robustness against interferences is evaluated using cyclo-stationary interference with a substantially large magnitude. The robustness against Gaussian and non-Gaussian noise is evaluated using Gaussian noise and alpha-stable noise, respectively.

6.2.1. *Case 1: The combined signals*

Some barriers need to be considered and understood to be able to use the proposed SM-IPSgram in practical applications. To this end, a distributed gear fault with a fault period of 1 order of the shaft speed, the spectral frequency of 3.5 kHz, the sampling frequency Δ_f of 50 kHz, and the duration of the signal of 4 sec (or 200 000 points) is simulated using the phenomenological gearbox model to mimic a distributed gear fault in practical applications. For the sake of comparison and to match the screen resolution for the SM-IPSgram estimation of the spectral log-mean-exp and ICS2gram, the same window lengths [2^n] and the 1/3-binary tree filter banks are used. The corresponding 1/3-binary trees are computed and displayed in Fig. 22. In the case of a single IFB, there is no need to design a weighting function because the results will be the same.

These results demonstrated that the proposed SM-IPSgram (see Fig. 22(a)) can accurately fulfil its mission of identifying rich IFB under harsh operating conditions. The SM-IPSgram effectively extracted the spectral frequencies of the distributed gear fault contained in the combined signals to get the earliest and most accurate diagnosis. This fact will not surprise those who recall that a whitened SM-IPS can is capable of attenuating strong background noises in the case where the signal-of-interest is phase-locked to a specific angular period. However, the SM-IPSgram estimation of the spectral log-mean-exp indicates that it will fail under heavy Gaussian noise.

On the other hand, the ICS2gram (see Fig. 22(b)) failed completely in the presence of cyclo-stationary interferences with a spectral frequency of 2 and 9 kHz. High ICS2 content at the first bandwidth (i.e. $f_{bw} = \Delta_f/2$) indicates that the method will fail under non-Gaussian noise. This obviously adheres to our intuition since the non-Gaussian noise cripples the performance of the squared envelope spectrum. It has become evident that there are definite limitations in the ICS2gram, like all methods of analysis, which greatly restrict its usefulness in gear diagnostics under harsh operating conditions.

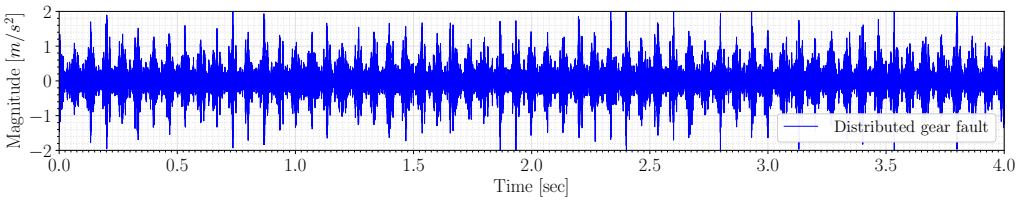

(a)

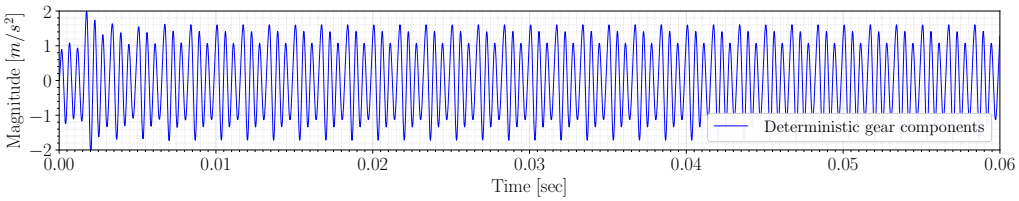

(b)

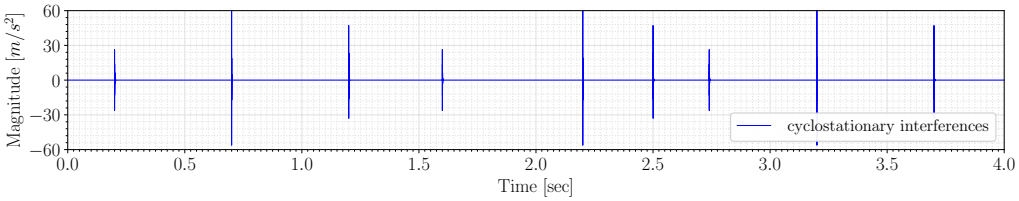

(c)

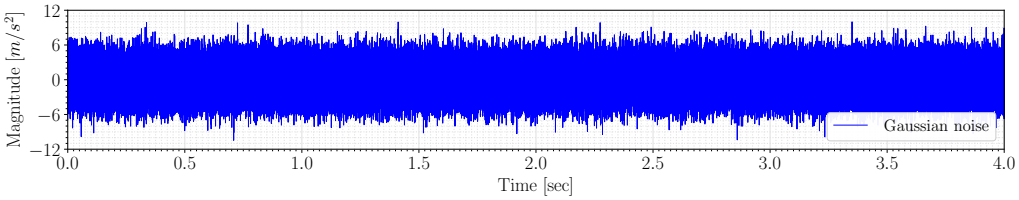

(d)

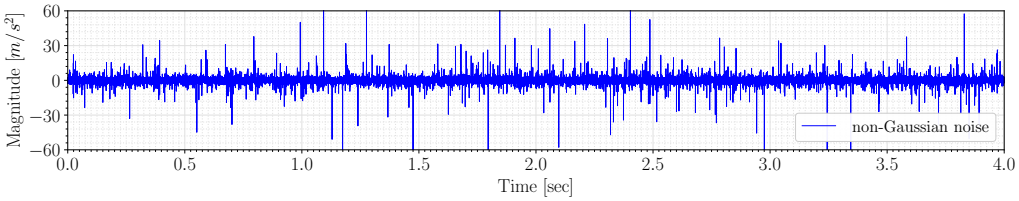

(e)

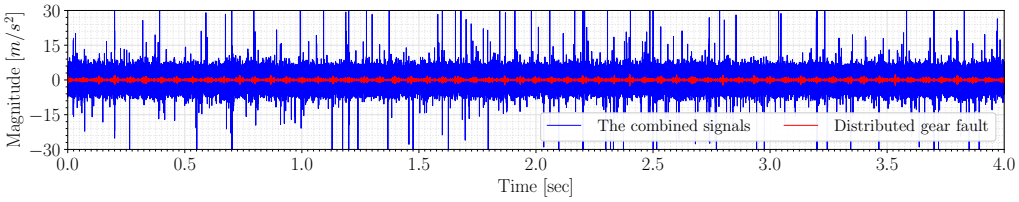

(f)

Figure 21: Phenomenological gearbox model: (a) distributed gear fault with a spectral frequency of 3.5 kHz, (b) zoomed-in view of the deterministic gear components in range [0, 0.06] sec, (c) random cyclostationary interferences with a spectral frequency of 2 and 9 kHz, (d) Gaussian noise with SNR = -17.53 dB, (e) alpha-stable noise with a stability index of $\alpha_n = 1.7$, and (f) zoomed-in view of the combined signals in the range [-30, 30]: (i) the combined signals (blue continuous line), and (ii) distributed gear fault (red continuous line).

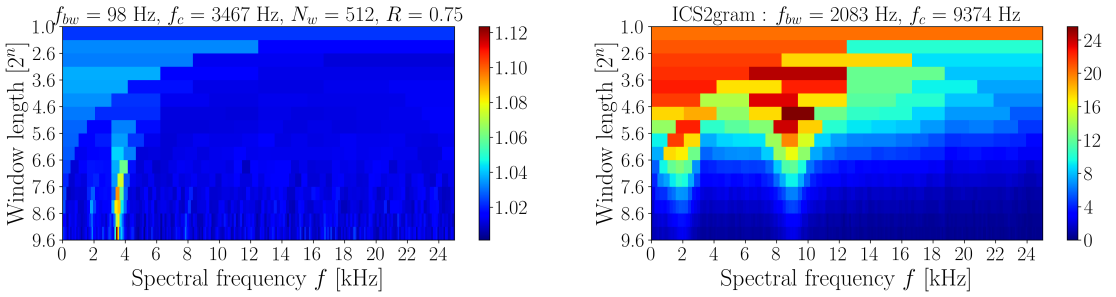

(a) (b)

Figure 22: Case 1: The combined signals (a) SM-IPSgram estimation of the spectral log-mean-exp, and (b) ICS2gram.

6.2.2. Case 2: Distributed gear fault + Gaussian noise (SNR = -17.53 dB)

In the previous subsection, the SM-IPSgram estimation of the spectral log-mean-exp has been demonstrated to provide consistently reliable guidance for identifying rich IFB. The efficiency of this method is believed to exceed most of the IFB identification methods (including the fast Kurtogram and the ICS2gram) when diagnosing gear faults in the presence of harsh operating conditions. Rather harsh operating conditions were purposely chosen to illustrate both the capabilities and superiority of the SM-IPSgram in gear diagnostics. In a similar way, we may use the SM-IPSgram again for motives of convenience to diagnose the distributed gear fault in the presence of Gaussian noise. Hence, the SM-IPSgram estimation of the spectral log-mean-exp, and the ICS2gram are computed and displayed in Figs. 23(a) and 23(b) respectively.

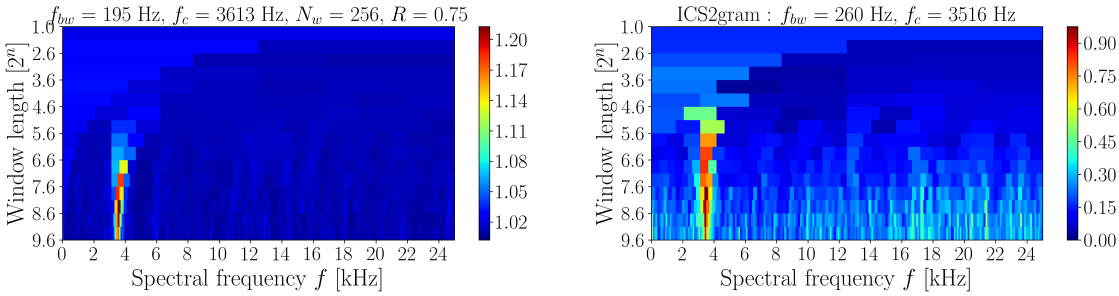

(a) (b)

Figure 23: Case 2: Distributed gear fault + Gaussian noise with SNR of -17.53 dB (a) SM-IPSgram estimation of the spectral log-mean-exp, and (b) ICS2gram.

As expected, the SM-IPSgram estimation of the spectral log-mean-exp (see Fig. 23(a)) effectually extracted the spectral frequency of the distributed gear fault in the presence of heavy Gaussian noise. In general, these SM-IPSgram show no significant perceptual differences when we compare the results in cases 1 and 2. For this specific case, the ICS2gram (Fig. 23(b)) is very informative and imposes no difficulty in the automatic identification of rich IFB. These results clearly indicate that most signal processing techniques perform sub-optimally in the presence of strong interferences and non-Gaussian noise.

A considerable number of observations would be necessary to determine whether the SM-IPSgram can be used for bearing diagnostics despite the bearing slip that worsens the method's performance. We propose to carry out some further investigations on the subject. Further investigations of the methods to remove the effects of the bearing slip on the whitened SM-IPS should be able to settle this question. A detailed paper by the authors on the SM-IPSgram for bearing diagnostics, together with a rigorous mathematical treatment of the binary tree resolution, will be published shortly. We also hope to show the performance of the spectral log-mean-exp for bearing diagnostics in a subsequent paper.

7. Conclusions

To conclude, the informative frequency band (IFB) in the presence of strong cyclo-stationary interferences, Gaussian and non-Gaussian noise is a difficult but important problem that often arises in many types of rotating machinery. The work presented in this paper is motivated by the need to perform gear diagnostics under these background noises. Hence, a new concept of spectral log-mean-exp sparsity measure was coined and the synchronous median instantaneous power spectrum-gram (SM-IPSgram) was proposed as an IFB identification method for gear diagnostics. The C-AIM (Centre for Asset Integrity Management) experimental

datasets and the phenomenological gearbox model have been used to demonstrate the performance of the SM-IPSgram with respect to the well-known fast Kurtogram and ICS2gram. The result of the comparison reveals that the proposed methods are effective in diagnosing the gear fault under harsh operating conditions. The SM-IPSgram is believed to be a very worthwhile IFB method for the following reasons: (i) it is computationally inexpensive, (ii) extremely robust, (iii) can cope with all kinds of background noises, e.g. strong interferences, Gaussian and non-Gaussian noise, and (iv) it produces a filter banks decomposition to accentuate only the carrier/spectral frequency of the defect.

References

[1] P. D. McFadden, J. D. Smith, Model for the vibration produced by a single point defect in a rolling element bearing, Journal of Sound and Vibration 96 (1) (1984) 69–82.

[2] P. D. McFadden, J. D. Smith, Vibration monitoring of rolling element bearings by the high-frequency resonance technique — a review, Tribology International 17 (1) (1984) 3–10.

[3] P. D. McFadden, J. D. Smith, The vibration produced by multiple point defects in a rolling element bearing, Journal of Sound and Vibration 98 (2) (1985) 263–273.

[4] G. Dalpiaz, A. Rivola, R. Rubini, Effectiveness and sensitivity of vibration processing techniques for local fault detection in gears, Mechanical Systems and Signal Processing 14 (3) (2000) 387–412.

[5] P. D. McFadden, Window Functions for the Calculation of the Time Domain Averages of the Vibration of the Individual Planet Gears and Sun Gear in an Epicyclic Gearbox, Journal of Vibration and Acoustics 116 (2) (1994) 179–187.

[6] R. Rubini, M. Sidahmed, Diagnostics of Gear Systems Using the Spectral Correlation Density of the Vibration Signal, IFAC Proceedings Volumes 30 (18) (1997) 971–976.

[7] J. Antoni, Fast computation of the kurtogram for the detection of transient faults, Mechanical Systems and Signal Processing 21 (1) (2007) 108–124.

[8] T. Barszcz, A. JabŁoński, A novel method for the optimal band selection for vibration signal demodulation and comparison with the Kurtogram, Mechanical Systems and Signal Processing 25 (1) (2011) 431–451.

[9] J. Antoni, R. B. Randall, The spectral kurtosis: application to the vibratory surveillance and diagnostics of rotating machines, Mechanical Systems and Signal Processing 20 (2) (2006) 308–331.

[10] J. Antoni, The spectral kurtosis: a useful tool for characterising non-stationary signals, Mechanical Systems and Signal Processing 20 (2) (2006) 282–307.

[11] D. Wang, P. W. Tse, K. L. Tsui, An enhanced kurtogram method for fault diagnosis of rolling element bearings, Mechanical Systems and Signal Processing 35 (1) (2013) 176–199.

[12] A. Moshrefzadeh, A. Fasana, The Autogram: An effective approach for selecting the optimal demodulation band in rolling element bearings diagnosis, Mechanical Systems and Signal Processing 105 (2018) 294–318.

[13] P. W. Tse, D. Wang, The design of a new sparsogram for fast bearing fault diagnosis: Part 1 of the two related manuscripts that have a joint title as "Two automatic vibration-based fault diagnostic methods using the novel sparsity measurement – Parts 1 and 2", Mechanical Systems and Signal Processing 40 (2) (2013) 499–519.

[14] P. W. Tse, D. Wang, The automatic selection of an optimal wavelet filter and its enhancement by the new sparsogram for bearing fault detection, Mechanical Systems and Signal Processing 40 (2) (2013) 520–544.

[15] J. Antoni, The infogram: Entropic evidence of the signature of repetitive transients, Mechanical Systems and Signal Processing 74 (2016) 73–94.

[16] W. A. Smith, R. B. Randall, X. du Mée, P. Peng, Use of cyclostationary properties to diagnose planet bearing faults in variable speed conditions, 10th DST group international conference on health and usage monitoring systems, 17th Australian aerospace congress (2017) 26–28.

[17] W. A. Smith, P. Borghesani, Q. Ni, K. Wang, Z. Peng, Optimal demodulation-band selection for envelope-based diagnostics: A comparative study of traditional and novel tools, Mechanical Systems and Signal Processing 134 (2019) 106303.

[18] S. Schmidt, A. Mauricio, P. S. Heyns, K. C. Gryllias, A methodology for identifying information rich frequency bands for diagnostics of mechanical components-of-interest under time-varying operating conditions, Mechanical Systems and Signal Processing 142 (2020) 106739.

[19] S. Schmidt, P. S. Heyns, K. C. Gryllias, An informative frequency band identification framework for gearbox fault diagnosis under time-varying operating conditions, Mechanical Systems and Signal Processing 158 (2021) 107771.

[20] A. Mauricio, W. A. Smith, R. B. Randall, J. Antoni, K. C. Gryllias, Improved Envelope Spectrum via Feature Optimisation-gram (IESFOgram): A novel tool for rolling element bearing diagnostics under non-stationary operating conditions, Mechanical Systems and Signal Processing 144 (2020) 106891.

[21] A. Mauricio, K. C. Gryllias, Cyclostationary-based Multiband Envelope Spectra Extraction for bearing diagnostics: The Combined Improved Envelope Spectrum, Mechanical Systems and Signal Processing 149 (2021) 107150.

[22] H. Oehlmann, D. Brie, M. Tomczak, A. Richard, Time-Frequency Analysis of Gearbox Faults, IFAC Proceedings Volumes 30 (18) (1997) 657–662.

[23] C. H. Page, Instantaneous power spectra, Journal of Applied Physics 23 (1) (1952) 103–106.

[24] W. J. Wang, P. D. McFadden, Early detection of gear failure by vibration analysis i. calculation of the time-frequency distribution, Mechanical Systems and Signal Processing 7 (3) (1993) 193–203.

[25] W. J. Wang, P. D. McFadden, Early detection of gear failure by vibration analysis–ii. interpretation of the time-frequency distribution using image processing techniques, Mechanical Systems and Signal Processing 7 (3) (1993) 205–215.

[26] J. Urbanek, T. Barszcz, R. Zimroz, J. Antoni, Application of averaged instantaneous power spectrum for diagnostics of machinery operating under non-stationary operational conditions, Measurement 45 (7) (2012) 1782–1791.

[27] J. Urbanek, T. Barszcz, J. Antoni, Time–frequency approach to extraction of selected second-order cyclostationary vibration components for varying operational conditions, Measurement 46 (4) (2013) 1454–1463.

[28] R. B. Randall, J. Antoni, Rolling element bearing diagnostics—A tutorial, Mechanical Systems and Signal Processing 25 (2) (2011) 485–520.

[29] N. Hurley, S. Rickard, Comparing Measures of Sparsity, IEEE Transactions on Information Theory 55 (10) (2009) 4723–4741.

[30] J. K. Baksalary, R. Kala, A bound for the euclidean norm of the difference between the least squares and the best linear unbiased estimators, The Annals of Statistics 6 (6) (1978) 1390–1393.

[31] R. E. Wendell, A. P. Hurter, Location theory, dominance, and convexity, Operations Research 21 (1) (1973) 314–320.

[32] J. K. Baksalary, R. Kala, A new bound for the euclidean norm of the difference between the least squares and the best linear unbiased estimators, The Annals of Statistics 8 (3) (1980) 679–681.

[33] P. O. Hoyer, Non-negative matrix factorization with sparseness constraints, Journal of Machine Learning Research 5 (2004) 1457 – 1469, cited by: 2191.

[34] C. Peeters, J. Antoni, J. Helsen, Blind filters based on envelope spectrum sparsity indicators for bearing and gear vibration-based condition monitoring, Mechanical Systems and Signal Processing 138 (2020) 106556.

[35] E. Mahmoudian, H. Amindavar, S. M. Ahadi, New sparsity measure based on energy distribution, Displays 80 (2023) 102542.
[36] K. Pearson, "Das Fehlergesetz und Seine Verallgemeinerungen Durch Fechner und Pearson." A Rejoinder, Biometrika 4 (1/2) (1905) 169–212.
[37] K. Pearson, On the curves which are most suitable for describing the frequency of random samples of a population, Biometrika 5 (1/2) (1906) 172–175.
[38] P. Lévy, Les lois de probabilitÉ dans les ensembles abstraits, Revue de Métaphysique et de Morale 32 (2) (1925) 149–174.
[39] P. Kruczek, R. Zimroz, J. Antoni, A. Wyłomańska, Generalized spectral coherence for cyclostationary signals with α-stable distribution, Mechanical Systems and Signal Processing 159 (2021) 107737.
[40] P. Borghesani, J. Antoni, CS2 analysis in presence of non-Gaussian background noise – Effect on traditional estimators and resilience of log-envelope indicators, Mechanical Systems and Signal Processing 90 (2017) 378–398.
[41] J. Wodecki, A. Michalak, A. Wyłomańska, R. Zimroz, Influence of non-Gaussian noise on the effectiveness of cyclostationary analysis – Simulations and real data analysis, Measurement 171 (2021) 108814.
[42] F. Combet, L. Gelman, Optimal filtering of gear signals for early damage detection based on the spectral kurtosis, Mechanical Systems and Signal Processing 23 (3) (2009) 652–668.
[43] J. Antoni, Cyclostationarity by examples, Mechanical Systems and Signal Processing 23 (4) (2009) 987–1036.
[44] D. Abboud, J. Antoni, S. Sieg-Zieba, M. Eltabach, Deterministic-random separation in nonstationary regime, Journal of Sound and Vibration 362 (2016) 305–326.
[45] T. Sibanda, S. Schmidt, Cyclomap: A new phase-cycle analysis to study the kinematics of gears and bearings, Mechanical Systems and Signal Processing 205 (2023) 110832.
[46] B. Hou, D. Wang, T. Xia, Y. Wang, Y. Zhao, K.-L. Tsui, Investigations on quasi-arithmetic means for machine condition monitoring, Mechanical Systems and Signal Processing 151 (2021) 107451.
[47] B. D. Ripley, Neural networks and related methods for classification, Journal of the Royal Statistical Society. Series B (Methodological) 56 (3) (1994) 409–456.
[48] S. Schmidt, S. P. Heyns, Normalisation of the amplitude modulation caused by time-varying operating conditions for condition monitoring, Measurement 149 (2020) 106964.
[49] A. Raad, J. Antoni, M. Sidahmed, Indicators of cyclostationarity: Theory and application to gear fault monitoring, Mechanical Systems and Signal Processing 22 (3) (2008) 574–587.
[50] C. J. Stander, P. S. Heyns, Instantaneous angular speed monitoring of gearboxes under non-cyclic stationary load conditions, Mechanical Systems and Signal Processing 19 (4) (2005) 817–835.
[51] D. H. Diamond, P. S. Heyns, A. J. Oberholster, Online shaft encoder geometry compensation for arbitrary shaft speed profiles using Bayesian regression, Mechanical Systems and Signal Processing 81 (2016) 402–418.
[52] D. Abboud, J. Antoni, S. Sieg-Zieba, M. Eltabach, Envelope analysis of rotating machine vibrations in variable speed conditions: A comprehensive treatment, Mechanical Systems and Signal Processing 84 (2017) 200–226.
[53] S. Schmidt, P. S. Heyns, K. C. Gryllias, A discrepancy analysis methodology for rolling element bearing diagnostics under variable speed conditions, Mechanical Systems and Signal Processing 116 (2019) 40–61.